Enigmatic high tenor Rh, Ru, Ir and Os-rich base metal sulfide mineralization within the Northern Limb of the Bushveld Complex: a product of fractionation of a sulfide liquid?

Kate R. Canham[1]*, David A. Holwell[1], Lara Du Preez[2], Paul Nex[3], Allan H. Wilson[3], Katie McFall[4], Erin S. Thompson[1], Hannah SR. Hughes[5], Andy Lloyd[2].

(1) Centre for Sustainable Resource Extraction, University of Leicester, University Road, Leicester, UK

(2) Anglo American South Africa, 144 Oxford Road, Rosebank, Johannesburg, South Africa

(3) School of Geosciences, University of the Witwatersrand, Johannesburg, South Africa

(4) Department of Earth Sciences, University College London, 5 Gower Place, London, UK

(5) Camborne School of Mines, Department of Earth and Environmental Sciences, University of Exeter, Penryn Campus, Penryn, Cornwall, UK

*Corresponding author: krc18@leicester.ac.uk

ORCID ID: Canham 0000-0001-7236-3140; Holwell 0000-0001-1023-7357; Thompson 0000-0001-8062-7126; McFall 0000-0001-8728-7822.

For the purposes of open access, the author has applied a creative commons attribution (CC BY) licence to any Author Accepted Manuscript version arising from this submission.

Author contributions: Conception and design, KC, DH, AL, HH; data collection and analysis, KC, AW; data contribution, AL, LD, AW, PN; paper writing and editing, KC, DH, KM, PN, ET.

Abstract

The Base Metal Zone (BM Zone) at Sandsloot in the Northern Limb of the Bushveld Complex, South Africa, is a highly unusual and high-grade Os-Ir-Ru-Rh, Fe-Ni-sulfide-rich horizon hosted within the deep Platreef, below the main PGE-horizon. The BM Zone ranges from 5 to 100 meters in thickness and is located up to 150 meters beneath the PGE-Reef. Base metal sulfide (BMS) mineralization occurs as disseminated/blebby to semi-massive/massive sulfides, with a typical assemblage of ~60/25/15 pyrrhotite/pentlandite/chalcopyrite modal%. The BM Zone is characterized by high (Os+Ir+Ru+Rh)/(Pt+Pd) ratios that reflect monosulfide solid solution (MSS) primitive mantle-normalized PGE profiles. The PGM assemblage is dominated by laurite (RuS_2) (62% by area) and IPGE+Pt arsenosulfides (21% by area). The PGE tenors of the sulfides vary between different textural styles, either reflecting R-factor variations or dilution of tenors by addition of crustal S. Disseminated/blebby sulfides have the highest tenors (up to 153 ppm Pd, 249 ppm Rh, 818 ppm Ru), whereas semi-massive/massive sulfides have lower tenors (up to 2.8 ppm Pd, 1.8 Pt ppm, 11 ppm Rh, 17 ppm Ru, 2.2 ppm Os, 3.5 ppm Ir).

The PGE geochemistry, IPGE-dominant PGM assemblage, abundance of Fe-sulfides, and high Ni/Cu ratios are consistent with the BM Zone representing the MSS portion of a sulfide liquid formed by fractional crystallisation. Furthermore, the Cu+Pt+Pd+Au-poor nature of the BM Zone suggests that these metals were removed from the BM Zone, and some Cu-rich veins and sections are present around the margins of Ni-Fe sulfide to support this. Increasing Pd/Ir and decreasing Rh/Cu ratios downhole indicate the sulfide liquid fractionated downwards. Therefore, a residual Cu-rich liquid, with associated Pt+Pd+Au, likely separated from MSS and was mobilised downwards and away from the BM Zone. Significantly, the mobilisation of a Cu-rich liquid leaves the possibility that an undiscovered Cu+Pt+Pd+Au orebody may exist at depth.

Introduction

The Northern Limb of the Bushveld Complex is best known for the Critical Zone hosted Platreef deposit, which is one of the largest PGE deposits in the world (Mudd et al., 2018). Within the Platreef, and PGE deposits more widely, palladium group elements-PPGE (Pt, Pd and Rh) typically display greater enrichment than iridium group elements-IPGE (Ru, Os and Ir). There are only a few rare occurrences where IPGE+Rh are dominant over Pt+Pd in sulfide-dominant ores. Examples include contact-style pyrrhotite-rich ores at the Creighton PGE deposit, Sudbury (Dare et al., 2010a), pyrrhotite-rich ores at Skalisty Mine, Norilsk-Talnakh (Tolstykh et al., 2022) and massive sulfides within the Eagle Ni-Cu-(PGE) deposit, Upper Michigan (Ding et al., 2012). These IPGE-rich ores all share a common theme – they are Fe-sulfide rich, massive to semi-massive sulfides.

Discontinuous massive sulfide mineralization in the shallow Platreef is known to occur at several locations, such as at the base of the unit at Tweefontein Hill (Nex, 2005) and Turfspruit (Sharman-Harris et al., 2005). Massive sulfides also occur within the footwall to the shallow Platreef at Overysel (Holwell and McDonald, 2006). More recently, drilling by Anglo American has identified disseminated to massive sulfide mineralization within the down-dip extension of the Platreef (hereafter referred to as the deep Platreef) at Sandsloot, Mogalakwena mine complex. This sulfide mineralization is located 10s to 100s of meters beneath the PGE-Reef, the shallow equivalent of which is the mined horizon.

The sulfide-associated ores in the deep Platreef at Sandsloot are IPGE-Rh-dominant over Pt-Pd and, thus, represent a new style of mineralization in the context of the Platreef. We describe this IPGE-Rh mineralization in the lower portions of the deep Platreef at Sandsloot for the first time, presenting textural mineralogy, geochemistry, and sulfide and platinum-group minerals (PGM) analyses. We compare the style and composition of this massive sulfide mineralization at Sandsloot to other occurrences within the Platreef, to demonstrate that the overall PGE contents are likely to be the product of variably fractionated and highly enriched sulfide liquid behaviour during emplacement.

Background

The Northern Limb of the Bushveld Complex

The 2.06 Ga (Zeh et al., 2015) Bushveld Complex, South Africa, hosts some of the world's largest magmatic sulfide deposits. It is divided into five geographically distinct limbs: the Western and Eastern Limbs host the UG-2 and Merensky Reef deposits, while the Northern Limb hosts the Platreef deposit (Cawthorn, 1999). The complex is comprised of the ultramafic-mafic Rustenburg Layered Suite, which intrudes into Paleoproterozoic sediments of the Transvaal Supergroup and Archean basement rocks. The Rustenburg Layered Suite is divided into five stratigraphic units: Marginal Zone norites, Lower Zone harzburgites and pyroxenites, Critical Zone chromitites, pyroxenites and norites, Main Zone gabbronorites, and Upper Zone anorthosites and gabbros and magnetites (Hall, 1932; Cawthorn, 1999).

The Northern Limb is a N-S-striking, westward-dipping sinuous outcrop extending over 120 km in length and 5 to 15 km in width. It is separated from the rest of the Bushveld Complex by the Thabazimbi-Murchison lineament (van der Merwe, 1976). The geology of the Northern Limb has been described extensively in numerous publications (e.g., van der Merwe, 1976; Maier et al., 2008; McDonald and Holwell, 2011; Kinnaird and Nex, 2015; Kinnaird and McDonald, 2018). It has mineralogical, stratigraphic and geochemical differences from the other limbs. As such, there is much debate as to whether it is directly correlatable with the rest of the Bushveld Complex south of the Thabazimi-Murchison lineament (e.g., McDonald et al. 2005; van der Merwe 2008; McDonald and Holwell 2011; Kinnaird and Nex 2015; Yudovskaya et al. 2017; Maier et al. 2021). The limb hosts significant PGE+Ni+Cu mineralization throughout its stratigraphy; however, the most extensively studied and economically mined is the Platreef deposit. The Platreef is overlain by the Main Zone and underlain by differing Paleoproterozoic sediments and Archaean gneiss/granite country rocks, or, in some locations, by the Lower Zone (Fig. 1). The footwall rocks to the Platreef become successively older moving northwards along strike. From south to north, the footwall rocks include the Timeball Hill-Magaliesberg Formation quartzites and shales, Duitschland Formation interbedded

limestones and tuffs, Penge Formation banded ironstones, Malmani Subgroup dolomites and limestones, and Archean granites and gneisses (van der Merwe 1976; Fig. 1).

The Platreef hosts a diverse range of Ni-Cu-PGE mineralization styles, including reef-style, disseminated and massive contact-style sulfides. The high variability in mineralization styles along the Platreef's strike is partly attributed to differing metamorphic, metasomatic and hydrothermal processes resulting from interaction with the highly heterogeneous footwall rocks (e.g., Harris and Chaumba, 2001; Armitage et al., 2002; Kinnaird et al., 2005; Holwell and McDonald 2006, 2007; McDonald et al., 2009; van der Merwe et al., 2012; Yudovskaya et al. 2017). Net textured and massive sulfides occur in the lower portions of the Platreef in several localities. At Tweefontein Hill (Fig. 1a), the development of massive sulfide mineralization, with an average thickness of 1.7 m, is thought to be related to the structure of the underlying footwall where sulfides accumulated in footwall depressions (Nex, 2005). In the Platreef at Turfspruit, minor massive and net-textured sulfides also occur towards the metasedimentary footwall (Hutchinson and Kinnaird, 2005; Kinnaird et al., 2005). In the Flatreef, the down-dip extension of the Platreef at Turfspruit (Fig. 1), 1 to 3 m thick massive sulfide pods occur beneath the PGE reef within a package of contaminated parapyroxenites, paraperidotites and calc-silicates (Yudovskaya et al., 2017). Net-textured and massive sulfides also occur within the gneiss footwall at Overysel (Fig. 1), these appear to have formed when fractionating sulfide liquid percolated downwards from the Platreef and accumulated in a partially molten footwall (Holwell and McDonald, 2007).

Recent research in and around the Mogalakwena Mine Complex in the Northern Limb

This work is part of a series of papers (see Thompson et al., 2025a; Thompson et al., 2025b; Thompson et al., *in review*; Canham et al., *in press*) presenting new data for the Northern Limb associated with extensive recent drilling conducted by Anglo American. These studies cover aspects of the magmatic emplacement and associated mineralisation in the Lower Zone and both shallow and deep Platreef at Tweefontein, Sandsloot, Zwartfontein and Overysel within

the Mogalakwena Mine Complex and adjacent exploration properties (Fig. 1a). A brief overview of these works is provided below for context.

Canham et al. (*in press*) describe the Zwartfontein Lower Zone chromitite-associated PGE+Ni+Cu mineralization, located north of Sandsloot (Fig. 1a). They propose a model in which localised carbonate and volatile assimilation triggered in situ chromite nucleation and sulfide saturation. Thompson et al. (2025a) use the Platreef as a case study to demonstrate the application of Niggli Numbers, comparing contamination signatures with Ni-Cu-PGE grade variations along strike of the Platreef (Tweefontein to Overysel; Fig. 1a). They suggest the deep Platreef at Sandsloot, and specifically the BM Zone which is the focus of this study, has some characteristics of a skarn-like system where carbonate assimilation may have acted to upgrade or generate PGE-Ni-Cu mineralization. Thompson et al. (2025b) focus on the magmatic history of the Platreef at Tweefontein, located south of Sandsloot (Fig. 1a), proposing a complex multi-sill emplacement model.

Most relevant to this study on the BM Zone at Sandsloot is Thompson et al. (*in review*), who give the first description of the stratigraphy of the deep Platreef at Sandsloot, using whole-rock geochemistry, silicate petrology, and silicate mineral chemistry to define several discreet units within the deep Platreef. The following stratigraphic framework for the deep Platreef at Sandsloot, defined by Thompson et al. (*in review*), is followed throughout this paper: (1) the Fly, (2) the PGE-Reef, which is the down-dip extension of the mined horizon, (3) the Sub-Reef and Sub-Reef Pyroxenite, (4) the Base Metal Zone (BM Zone), and (5) the Sub-Base Metal Zone (Sub-BM Zone) (Fig. 1b). The uppermost unit of the deep Platreef, the Fly, is characterised by homogeneous feldspathic pyroxenites with limited carbonate contamination. Underlying this is the PGE-Reef, which is the most Pt+Pd-enriched portion of the deep Platreef and is characterised by altered feldspathic pyroxenites that are highly carbonate contaminated. Beneath the PGE-Reef is the Sub-Reef, which is lithologically similar to the PGE-Reef and highly carbonate contaminated, but lacks significant PGE mineralization. The BM Zone is characterised by pegmatoidal feldspathic clinopyroxenites. It is sulfide+PGE-rich

and also highly carbonate contaminated. The transition from the BM Zone into the underlying Sub-BM Zone is marked by the return to feldspathic pyroxenites, with orthopyroxene as the dominant mineral (Thompson et al., *in review*).

In this contribution, we specifically examine the ore mineralogy of the BM Zone at Sandsloot and its newly recognised IPGE+Rh-rich nature, presenting details on the metal tenors, and PGE and sulfide mineralogy for the first time.

Sampling and analytical methods

Drill cores SSAA019, SSAA043, SSAA034, SSAA029 (SA19, SA43, SA34, SA29) (Fig. 1) were selected for sampling. These drill cores were selected as they intersect a range of sulfide textures and Cu+Ni+PGE grades. Twelve quarter core samples of 30-50 cm were sampled from the BM Zone, three additional samples were taken from above and below the BM Zone in SA43 (Table 1). Thin sections were prepared from these samples at the University of Leicester and the remaining material was crushed and milled using steely fly press and agate ball mills in preparation for bulk rock geochemical analysis.

Geochemistry

Whole-rock metal grades are discussed as ratios and relative terms only throughout the manuscript due to commercial sensitivity. Bulk rock major element oxide geochemistry of ~1-meter intervals downhole, alongside Cu, Ni, Pt, Pd, Co and Au assays were provided by Anglo American. Rhodium assays were available when Pt+Pd values were over a certain threshold (>1 ppm). Major elements were undertaken on glass discs produced by borate fusion followed by X-ray fluorescence (XRF); the trace elements Cu+Ni+Co through pressed pellet XRF; and PGE+Au through Pb fire assay with ICP-OES finish at SGS Laboratories, South Africa. The additional 15 quarter core samples selected for this study were analysed for trace elements by XRF on pressed powder pellets at the University of Leicester and by four-acid digestion with inductively coupled plasma atomic emission spectroscopy (ICP-AES) (ALS method code: ME-ICP61) at ALS Geochemistry, Loughrea, Ireland. Reference materials (OREAS

141/137/924/195, MRGeo08, EMOG-17) were analysed to monitor data quality. The percentage relative difference (RD%) of the relevant trace elements range from 1.6 to 7.8% and percentage relative standard deviation (RSD%) from 0 to 4.3%, classified as very good following Piercey (2014). A subset of samples (n=6) was analysed for full 6PGE (Os, Ir, Ru, Rh, Pt, Pd) geochemistry by Ni sulfide fire assay with inductively coupled plasma-mass spectrometry (ICP-MS) (ALS method code: PGM-MS25NS) by ALS Geochemistry, Johannesburg. Standards OREAS684/683 and AMIS0498 alongside blanks and repeats were also run. The %RD and %RSD range from 2.5-9.4% and 0-4.3%, respectively.

Intersections of net-textured sulfides from the shallow Platreef at Tweefontein Hill (Fig. 1a) were sampled from TN190D1 (Appendix Figure A1). These were used for comparison of PGE+Ni+Cu patterns between the BM Zone and semi-massive sulfides elsewhere in the Platreef. Samples were crushed and milled for bulk rock analysis and analysed for 6PGE+Au by Ni-S fire assay followed by ICP-MS at the School of Geosciences, University of KwaZulu Natal (whilst lab was under supervision of A.W). International reference materials SARM6 and SARM7, alongside repeats were analysed. Copper and Ni were determined through pressed pellet XRF (error ranges from 0.3-1.1 %). Full details of the limits of detection, alongside accuracy and precision estimates for all whole-rock geochemical analysis are available in Table. A1.

Trace elements in sulfides

The concentration of trace elements in sulfide was established by laser ablation inductively-coupled plasma mass spectrometry (LA-ICP-MS) analysis at the University of Leicester, using a ThermoScientific ICAP-Qc quadrupole ICP mass spectrometer, equipped with a New Wave Research-ESI 213nm laser unit, following methods outlined in Barnes et al. (2020); Tolstykh et al., (2022); Blanks et al. (2022). Track ablations were performed at a spot size of 50 μm, laser frequency of 5 μm, pulse rate of 10 Hz and fluence of 3.5-4 J/cm^2. Total acquisition lasted 90-120 s, including 30 s of gas background prior to ablation. The following isotopes were measured: ^{28}Si, ^{29}Si, ^{33}S, ^{47}Ti, ^{49}Ti, ^{53}Cr, ^{57}Fe, ^{59}Co, ^{60}Ni, ^{61}Ni, ^{63}Cu, ^{66}Zn, ^{68}Zn, ^{75}As, ^{77}Se, ^{82}Se,

^{101}Ru, ^{103}Rh, ^{105}Pd, ^{107}Ag, ^{108}Pd, ^{121}Sb, ^{125}Sb, ^{185}Re, ^{189}Os, ^{193}Ir, ^{195}Pt, ^{197}Au, ^{208}Pb, ^{209}Bi. Data reduction was carried out using iolite v.4 software. To mitigate the effect of ablating any micro inclusions, SEM surveys were carried out prior to LA-ICP-MS analyses to identify any visible micro inclusions. Time resolved analysis (TRA) spectra were also monitored and any PGM micro inclusions were manually excluded. Additionally, Cr, Ti and Si were monitored to ensure no silicate or oxides were included in the analyses.

Calibration was carried out using UQAC-FeS1 on ^{33}S (Holwell et al., 2015; McFall et al., 2019). This was measured between changing samples and every 20-30 minutes during analysis to account for any instrument drift. To check for interferences multiple isotopes for elements were collected. It is known that ^{105}Pd is interfered by ^{65}Cu^{40}Ar; therefore, we used ^{108}Pd. ^{108}Pd is interfered by ^{68}Zn^{40}Ar, and ^{108}Cd, so ^{68}Zn and ^{108}Cd were monitored. For pyrrhotite and pentlandite Zn and Cd concentrations were both low (below 10 ppm), so no correction was needed. However, Zn was very high in chalcopyrite (up to 1007 ppm) resulting in significant interferences on ^{108}Pd; thus, no Pd concentrations are reported for chalcopyrite. ^{103}Rh is interfered by ^{63}Cu^{43}Ar, so no ^{103}Rh values are reported for chalcopyrite. To monitor results MASS-1 was measured when changing samples and at the beginning and end of the day. The %RSD and %RD of PGE range from 6.2 to 9.8% and 5.6 – 11.0%, respectively (full accuracy and precision are given in Appendix Table. A2 and detection limits in Appendix Table. A4).

PGM Studies

Seven thin sections were analysed for PGM by Energy-Dispersive X-ray Spectroscopy (EDS) analysis using a ZEISS Sigma field emission scanning electron microscope (SEM) equipped with two Bruker 6l30 EDX detectors at the University of Leicester. The thin sections were chosen based on their assay grade and sulfide textures to ensure a spread of samples throughout the BM Zone. Samples were mapped using the automated mapping software ZEISS Mineralogic. The sample run conditions were set to a magnification of 250-500x, step size of 1 μm^2, dwell time of 0.25 secs, accelerating voltage of 20 kV, and aperture of 120 μm. As PGM and PMM have a high specific gravity they appear bright under backscattered

electron (BSE) imaging relative to sulfides and silicates; therefore, a bright phase threshold was established so any phases (PGM and PPM) over the assigned brightness threshold would be identified and mapped. Additionally, the area to be mapped was dilated by 3x to incorporate the surrounding host mineral and gain information on each PGM's association. During analysis, the area (μm^2), Feret max diameter (μm) and semi-quantitative composition (wt.%) of each PGM was recorded. The measured stoichiometric values were then used to assigned each PGM a name from a custom-designed PGM library. After the automated analysis, PGMs were individually revisited manually to gain broader association data and collect high quality photomicrographs.

Mineral Maps

The same 7 thin sections analysed for PGM were also analysed by automated, quantitative SEM mapping to produce mineral maps using ZEISS Mineralogic software (Holwell et al., 2017). The remaining thin sections were assessed optically to ensure findings are consistent across the samples. The analysis was performed at operating conditions of 20 kV, a working distance of 8.5 mm and an aperture of 120 μm. A dwell time of 0.05 secs and a step size of 25-40 μm^2, varying depending upon grain size, was utilised. Counts for EDS detection were consistently above 3000.

Stratigraphy

The BM Zone is located in the deep Platreef at Sandsloot. We use the term deep Platreef throughout this study to refer to the rocks that occur between Main Zone and the metasedimentary footwall or Lower Zone (Fig. 1). In the deep Platreef at Sandsloot PGE+Ni+Cu mineralization is contained within two key horizons: (1) the PGE-Reef, the shallow equivalent of which is the mined horizon and (2) the BM Zone, which is the focus of this study. Footwall rocks have, as of yet, not been intersected below the deep Platreef at Sandsloot.

The BM Zone lies ~50 to ~150 meters beneath the PGE-Reef. The relative proportion of Ni, Cu, Pt+Pd within the BM Zone compared to the overlying PGE-Reef is outlined in Figure 2a for drillholes SA43 and SA19, which are considered representative of the BM Zone (logs for additional holes sampled are provided in Appendix Figure A1). The BM Zone is variably developed, ranging in thickness from 5 m (e.g., in SA43) to ~100 m (e.g., in SA19). The intensity of Ni-Cu-PGE sulfide mineralization within the BM Zone is also highly variable; sulfides occur as disseminated/blebby sulfides only in some holes (e.g., SA43, SA34; Fig. 2b), while other holes intersect semi-massive/massive sulfides (SA19; Fig. 2a). Above and below the BM Zone are a series of pyroxenites and feldspathic pyroxenites that can be highly altered.

Petrology

To conform to previous studies of the Northern Limb (e.g., Harris and Chaumba, 2001; Armitage et al., 2002; McDonald et al., 2005; Holwell et al., 2006) we follow general Bushveld nomenclature. Therefore, we use the terms feldspathic clinopyroxenites and pegmatoidal feldspathic clinopyroxenites, even though these rocks would be instead be classified as gabbronorites and gabbros under the IUGS classification. Here we describe the petrology of the rocks that host the disseminated to blebby and semi to massive sulfides of the BM Zone at Sandsloot. Further details on the geochemistry and nature of this unit within the broader stratigraphy at Sandsloot can be found in Thompson et al. (*in review*).

The BM Zone at Sandsloot is comprised of pegmatoidal feldspathic clinopyroxenites (with a notable absence of orthopyroxene, which is generally the dominant pyroxene in Platreef rocks), pegmatoidal clinopyroxenites, feldspathic clinopyroxenites and massive sulfides. *Pegmatoidal feldspathic clinopyroxenites* (Fig. 2) are comprised of coarse-grained plagioclase (40-60 modal%) and clinopyroxene (40-60 modal%; Fig. 3a). Plagioclase tends to form coarse-grained laths (up to 2 cm) and is extensively altered to prehnite (Fig. 3a, b), clinopyroxene may also be coarse-grained (up to 0.5 cm) or medium- to fine-grained (0.5- 2 mm) and subhedral (Fig. 3b). *Feldspathic clinopyroxenites* are comprised of clinopyroxene (50-85 modal%), plagioclase (15-50 modal%) and minor orthopyroxene (<10 modal%). Fine-

grained (0.1-0.5mm) clinopyroxene and plagioclase can form an amoeboid granoblastic texture (Fig. 3b) or irregular coarser grains. *Pegmatoidal clinopyroxenites* are comprised of clinopyroxene (85-90 modal%) and plagioclase (<15 modal%). Clinopyroxene is typically coarse-grained (up to 1.5 cm) with fine grained intergrowths of plagioclase (Fig. 3c). Sections of finer grained subhedral clinopyroxene (0.5-2 mm) with interstitial plagioclase are also present. *Massive sulfides* are described in the subsequent section. They occur where sulfide comprises >80 modal% of the rock, with lesser clinopyroxene, plagioclase and Fe-oxides.

Accessory minerals seen in all lithologies include magnetite, ilmenite and apatite. Disseminated ilmenite and magnetite (<1 modal%) are common in association with disseminated/blebby sulfides, and where semi-massive to massive sulfides are present magnetite+ilmenite is often more abundant (0-15 modal%). Calcite is also commonly observed, and often this is associated with sulfide (Fig. 3e).

The rocks within the BM Zone have experienced variable degrees of alteration. In addition to the prehnite alteration of plagioclase, clinopyroxene can be partially to completely altered to talc. Where alteration is more extensive, phlogopite and hornblende occur as accessory phases, along with extensive chlorite and serpentine (Fig. 3f).

Sulfide mineralogy

Sulfide mineralization in the BM Zone at Sandsloot is present as disseminated to blebby, vein, semi-massive (including net-textured) and massive sulfides. On the whole, sulfides are predominately pyrrhotite, with lesser pentlandite and chalcopyrite, in an average modal% of ~60/25/15 pyrrhotite/pentlandite/chalcopyrite. A summary of the sulfide textures for each sample is provided in Table. 1.

Semi-massive to massive sulfides

Pyrrhotite is the dominant sulfide within massive/semi-massive sulfides, followed by pentlandite, with lesser chalcopyrite. Pentlandite is present as loops around pyrrhotite (Fig. 4a, c), exsolution flames within pyrrhotite and along fractures within pyrrhotite (Fig. 4b).

Chalcopyrite is typically separated and restricted to the boundaries of the semi-massive/massive sulfides (Fig. 4c) and is also present in Cu-rich sulfide veins at the peripheries of Fe-Ni sulfide patches (Fig. 4d).

In massive/semi-semi-massive sulfides a common texture within pegmatoidal clinopyroxenites is coarse-grained sulfide-clinopyroxene symplectites (Fig. 4c, e). Surrounding the sulfide symplectite are worm-like intergrowths of plagioclase, sulfides ± magnetite, ilmenite and clinopyroxene (Fig. 4e). In pegmatoidal feldspathic clinopyroxenites sulfides are typically net textured and networks of sulfides are distributed between coarse plagioclase laths (Fig. 4f). Net textured sulfides are grouped under semi-massive/massive sulfides.

Magnetite is present along fractures within sulfides and also occurs as coarse-grained, subrounded inclusions (up to 3 mm) with ilmenite within sulfide (Fig. 4g). Calcite inclusions are common in massive sulfides and are often rimmed by chalcopyrite (Fig. 4b).

Disseminated to blebby sulfides

Blebby sulfides (<10 modal% sulfide) are up to 1 cm, predominately pyrrhotite with pentlandite rims (Fig. 5a). Minor chalcopyrite may also be present within the rims; however, chalcopyrite tends to form separate, smaller sulfide blebs (<2 mm) that are chalcopyrite-dominant, with pyrrhotite and pentlandite around their boundaries. Calcite blebs are commonly found within the chalcopyrite-dominant sulfides (Fig. 5a, c). As with the massive sulfides, magnetite often occurs along sulfide fractures.

Vein sulfides

Coarse-grained sulfide veins (Fig. 5d-e), up to 1 cm thick, are typically associated with highly altered lithologies, where abundant chlorite and accessory phlogopite and hornblende is present. Fine-grained sulfide veins (<0.1 mm) are often chalcopyrite dominant (Fig. 5f-g). Sulfide veins typically also contain calcite. Sulfide veins with pentlandite and pyrrhotite separated from chalcopyrite are also noted in intersections of massive sulfide (Fig. 4d).

Whole-rock geochemistry

Downhole geochemistry

Selected whole-rock geochemistry and ratios of samples from this study are provided in Table. 2. Figure 6 shows the downhole variation of base and precious metals (Ni, Cu, Pt, Pd, Co, Au), as well as CaO, MgO, Al_2O3, Fe_2O_3 and TiO_2 through two drillholes that intersect the BM Zone: the first intersecting semi-massive/massive sulfide mineralization (Fig. 6a) and the second intersecting disseminated to blebby sulfides (Fig. 6b). Downhole geochemical logs for the additional holes sampled are available in Figure A1.

In the drillhole containing intersections of semi-massive/massive sulfides (Fig. 6a), two significant intersections of semi-massive to massive sulfides occur, from 724-731 m and 745-758 m. Above and in between these two zones disseminated/blebby sulfides are present; as such, Ni and Cu are still elevated, but to lesser extent. High abundances of Fe_2O_3 and S correlate with zones of massive sulfide, with S ranging from 7 wt.% in semi-massive sulfides up to 34 wt.% in massive sulfides (Table. 2). Increases in Al_2O_3 (up to 15 wt.%) relate to increase in the modal proportion of plagioclase and prehnite after plagioclase. High CaO contents (>10 wt.%) reflect the abundance of clinopyroxene, and low MgO contents (<10 wt.%) are due to the lack of olivine and orthopyroxene. Below the BM Zone, the Sub-BM Zone is marked by an increase in MgO (15-40 wt.% MgO) as serpentinised pyroxenites and harzburgites become more dominant. Bulk TiO_2 is very low (<0.02 wt.%) in the first massive sulfide intersection, but increases in the second massive sulfide intersection to 0.2 to 0.7 wt.%. The Cr_2O_3 contents are consistently low (<0.02 wt.%) within the BM Zone. Granitic intersections are present in places and correlate with CaO/Al_2O_3 decreases (<0.5) and SiO_2 increases.

In drillholes containing blebby and disseminated sulfides (as exemplified by the drillhole intersection in Fig. 6b) the BM Zone can vary in thickness, ranging from 5 m (e.g., SA43; Fig. 6b) to 110 m (e.g., SA56). Sulfur concentrations range from 0.8 to 2.7 wt.% (Table. 2). As in

the semi-massive/massive sulfides, MgO decreases from the unit above into the BM Zone (<10 wt.%), while Al_2O_3 (>10 wt.%) and CaO (>11 wt.%) increase, reflecting an increase in the proportion of clinopyroxene and plagioclase in the BM Zone. Unlike the semi-massive/massive sulfides, Fe_2O_3 decreases from the unit above, due to the increase of plagioclase, reduction in pyroxene and olivine, and lesser amount of sulfide (Fig. 6b).

Chalcophile element geochemistry

Copper and Ni grades are controlled by the amount of sulfide. Nickel and Cu reach high and moderate grades, respectively, in intersections of semi-massive/massive sulfides (Fig. 6a), and lower grades in blebby/disseminated sulfides (Fig. 6b). Within intersections of blebby/disseminated sulfides (Fig. 6b) Pt+Pd grades range from moderate to high, whilst IPGE and Rh abundances are very high, and Co is up to 261 ppm. In contrast, Pt and Pd are low within the semi-massive/massive sulfides (Fig. 6a), whilst IPGE+Rh are higher, as is Co (up to 1480 ppm). The (Os+Ir+Ru+Rh)/(Pt+Pd) ratio within the BM Zone ranges from 0.6 to 22.4 (average 9.6).

Within the semi-massive/massive sulfides Ni/Cu ratios average 5.4, ranging from 2 to 20 (Fig. 7a). Platinum and Pd broadly correlate, showing a strong correlation in intersections of semi-massive/massive sulfides (Fig. 7b); at lower Cu and Ni concentrations peaks of Pt and Pd may be offset downwards by several meters relative to Cu and Ni (Fig. 6a). The Pt/Pd ratio ranges from 0.2 and 0.7, and Pd/Ir ratios from 0.35 to 0.73, aside from a sample from the very base of BM Zone which has a Pd/Ir ratio of 20.8 (Table. 2). Peaks in Co correlate strongly with Ni and Cu (Fig. 6a, 7c), whilst Au shows a weaker correlation with PGE, Cu and Ni (Fig. 6a, 7d). The S/Se ratios range from 5702 to 8393 (Table. 2).

Where the BM Zone is developed as disseminated/blebby sulfides (Fig. 6b), as opposed to massive sulfides (Fig. 6a), Ni/Cu ratios are generally lower (average 2.2), whilst Pt/Pd (0.7 to 1.4) and Pd/Ir (1.22) ratios are higher. As with the semi/massive to massive sulfides, Co, Pt,

Pd and Rh broadly correlate with Ni and Cu, whilst Au shows a weaker correlation (Fig. 6b, 7d). The S/Se ratios range from 2000 to 6361 (Table. 2).

Cu, Ni and PGE tenors

The concentration of Ni, Cu and PGE in 100% sulfide (i.e. metal tenors) was calculated applying the method of Barnes and Lightfoot (2005) and is outlined in Table 3. Samples containing <0.2 wt.% S were excluded from the calculations. In line with our petrographic assessment, we assume that the sulfide mineralogy is pentlandite, pyrrhotite and chalcopyrite. The Ni tenors are variable between 5.5 and 14.3 wt.%. Semi-massive/massive sulfides have lower Ni tenors (4.9 to 9.2 wt.%) than disseminated to blebby sulfides (6 to 14.3 wt.% Ni). Copper tenors are more restricted than Ni, with all semi-massive/massive sulfides having consistently low Cu tenors (0.3 to 1.7 wt.%), whilst disseminated/blebby sulfide tenors are higher (2 to 7.9 wt.% Cu).

Platinum, Pd and Rh tenors are variable. Disseminated/blebby sulfides range from 4 to 153 ppm Pd, 3 to 174 ppm Pt and 3 to 249 ppm Rh, whilst semi-massive/massive sulfides tenors are more consistent between 0.9 to 2.8 ppm Pd, 0.3 to 1.8 Pt ppm and 0.9 to 11 ppm Rh. The IPGE tenors of semi-massive/massive sulfides are up to 2.2 ppm Os, 3.5 ppm Ir and 17.3 ppm Ru. The IPGE tenors of disseminated/blebby sulfides are only available for one sample, but are significantly higher; Os, Ir and Ru tenors are 81, 126 and 818 ppm.

Primitive mantle normalized metal profiles

Primitive mantle-normalized whole-rock patterns for the BM Zone, displayed by sulfide texture, are shown in Figure 8a. The sample of disseminated/blebby sulfides shows distinctive enrichment in IPGE+Rh. It has a positive slope between Os to Rh and a steeply decreasing slope from Rh through to Au. The semi-massive/massive sulfides also show enrichment in IPGE+Rh relative to Pt, Pd and Au, seen by an extreme negative slope from Rh through to Pt, followed by a steady increase in the profile from Pt to Cu. One semi-massive/massive sulfide sample, containing the highest Cu and Ni, has a different profile to the other samples. It

exhibits a positive slope from Os all the way through to Cu; however, it displays an extreme positive Rh anomaly. The overlying PGE-Reef in the deep Platreef at Sandsloot is plotted on Figure 8a for comparison. The BM Zone is anomalously low in Pt, Pd and Au, but enriched in IPGE+Rh, compared to the PGE-Reef.

On Figure 8b primitive mantle-normalised PGE patterns are shown for semi-massive/massive sulfides that occur towards the base of the shallow Platreef at Tweefontein Hill (Nex, 2005). Their profile shows a positive slope from Os through to Cu, but with an extreme negative Au anomaly. Excluding the negative Au anomaly the shape of the PGE profile at Tweefontein Hill is similar to the PGE-Reef in the deep Platreef at Sandsloot; however, PGE is an order of magnitude lower, while Ni and Cu are higher. When compared to the BM Zone, the Tweefontein Hill profile shows a positive profile from Os through to Pd. In contrast, the BM Zone shows a positive profile from Os to Rh, followed by a very steep negative profile from Rh to Pd or Pt, which then flattens to Au. The concentrations of Ni can be significantly higher in the BM Zone at Sandsloot than Tweefontein Hill, while the Cu concentrations are comparable.

Trace elements in sulfide

Summary statistics of the trace element concentrations for the different sulfide styles and minerals is provided in Table 4. A selection of trace element contents in pentlandite and pyrrhotite is also displayed in Figure 9.

Across the sulfide styles pentlandite generally contains the highest concentrations of Rh, Pd and Co, while both pyrrhotite and pentlandite contain similar concentrations of Ru, Os and Ir. Chalcopyrite generally contains no appreciable PGE (Table. 4).

When comparing the sulfide styles blebby/disseminated sulfides contain higher Pd, Ru and Rh in pentlandite than semi-massive/massive sulfides. The Rh and Ru concentrations can reach up to 244 ppm and 45 ppm, respectively, in blebby/disseminated pentlandite (Fig. 9a-c). In contrast, the Os and Ir concentrations of pentlandite and pyrrhotite are comparable in

both disseminated/blebby and semi-massive/massive sulfides (Fig. 9d, e). Semi-massive/massive sulfides contain no Pt in solid-solution, but notably, blebby/disseminated pentlandite can contain up to 4.2 ppm Pt (Table. 4). The PGE contents in vein sulfides appear to mirror that of either the disseminated/blebby sulfide or semi-massive/massive sulfide with which they are spatially associated. Two vein samples were analysed. One sample, a sulfide-calcite vein in the Sub-BM Zone, has similar high Pd and Rh contents in pentlandite to overlying disseminated/blebby sulfides from the same drill hole. The second, a Cu-rich fractionated vein associated with a zone of semi-massive/massive sulfides, has significantly lower Pd and Rh contents within pentlandite, comparable to the semi-massive/massive sulfides with which it is spatially associated.

Platinum Group Mineralogy

A total of 240 grains of precious metal minerals, totalling 57,007 μm^2, were identified from the seven thin sections analysed (Table 5; full results available in Table. A5, A6). One blebby sulfide sample contained several very coarse PGM (each >5000 μm^2); therefore, results are presented as both number of grains and relative area. Platinum-group minerals were grouped into the following categories: (1) Ru-S, (2) Ir-As, (3) IPGE+Pt-As-S, (4) Ir-alloys, (5) PPGE-As, (6) Pt-Bi-Te, (7) Pd-Bi-Te, (8) Pt-Fe and (9) Au-Ag (Table. 6). A summary of the PGM groups, with PGM names and ideal formulas is given in Table 5.

By number of grains, Ru-S (27%), Ir-As (20%), IPGE+Pt-As-S (16%) and Au-Ag (15%) are the most common PGMs and PMMs. The Pt-Fe (9%), PPGE-As (6%) and Pt-Bi-Te (6%) are less abundant, while Pd-Bi-Te and Ir-alloys comprise <1% each (Fig. 10). By % of PGM by area, Ru-S is the most dominant PGM (62%), followed by IPGE+Pt-As-S (21%), Pt-Fe (11%) and Au-Ag (3%). The Ir-As, Pt-Bi-Te, Pd-Bi-Te, Ir-alloys and PPGE-As make up <1% of PGM by area each (Fig. 10).

The PGM were also classified according to their association with surrounding minerals (Fig. 11a). The majority of PGMs have a close association with base metal sulfides (Fig. 11b-h): Ir-

As (Fig. 11c), Ir-alloys and Pt-Pd-Bi-Te are hosted exclusively by sulfide or on sulfide boundaries. The Ru-S, IPGE+Pt-As-S, and Au-Ag are found predominately hosted within (23 to 33% of grains) or on sulfide boundaries (25-57% of grains) (Fig. 11d-g), while less commonly they are hosted within secondary silicates (10-31% of grains) (Fig. 11h). Conversely, the Pt-Fe and PPGE-arsenides are often hosted within secondary silicates, such as prehnite and serpentine (67% of PPGE-As and 39% of Pt-Fe grains), although a portion of these are associated with sulfide (Fig. 11a).

Mass Balance

Six samples with full bulk rock PGE geochemistry, in situ LA-ICP-MS sulfide analyses and PGM data available were selected for mass balance calculations. These included four semi-massive/massive sulfide samples, one Cu-rich fractionated sulfide vein, and one blebby sulfide sample. To establish the percentage of each PGE contained within each sulfide ($P_{\mathrm{Sul}}i$), the equation of Godel et al. (2007) was utilised:

$$\left(P_{Sul}{}^{i}\right) = \left(F_{Sul} C_{Sul}{}^{i} / C_{WR}{}^{i}\right) x\ 100$$

Where F_{Sul} is the relevant sulfide weight fraction, C_{Sul} is the concentration of the element i (either Pt, Pd, Rh, Ru, Ir, Os) in the sulfide and C_{WR} is the concentration of the element i in the whole-rock (Godel et al., 2007). Full results are available in Table. A7.

Palladium is always accounted for in total sulfide, predominately pentlandite, and this is in agreement with our PGM analysis, in which only 0.2% of the total PGM area were Pd dominant. Palladium in sulfide is slightly overestimated (ranging from 108-121%); however, overestimations have also been reported in other deposits where Pd is accounted for totally in pentlandite (e.g., Osbahr et al. 2013). In contrast to Pd, almost no Pt is contained within sulfide. All massive/semi-massive sulfides contain no Pt in sulfide, while blebby sulfides can contain up to 0.7% of total Pt in pentlandite (Fig. 12).

A sample of a Cu-rich fractionated sulfide vein (Table 1) contained a lower proportion of IPGE+Rh within sulfide compared to the other semi-massive/massive sulfides. Total sulfide

hosts <2% of IPGE+Rh. Within the remaining semi-massive/massive sulfides, the proportion of Rh contained within sulfide is variable, ranging from 19-64 %. The Ru, Os and Ir proportions range from 55-100%, 10-100% and 29-80% in total sulfide, respectively. The blebby sulfide sample only contains 3.0, 2.3 and 0.6% Ru, Os and Ir in total sulfide, which is in agreement with the abundance of Os-Ir-bearing laurite and IPGE+Pt-As-S observed in this sample (Fig. 11e, g).

Discussion

The BM Zone in the deep Platreef at Sandsloot is a sulfide-rich zone that lies 50 to 150 meters beneath the PGE-Reef. The most important features identified in this study, which require explanation, are:

1. High IPGE+Rh, resulting in (IPGE+Rh)/(Pt+Pd) ratios ranging from 0.6 to 22.4 (mean 9.6) and Pd/Ir ratios generally <1.5, as well as high Ni/Cu ratios (1.1 to 21.6).
2. High but variable PGE tenors within disseminated/blebby sulfides (4 to 153 ppm Pd, 3 to 174 ppm Pt, 249 ppm Rh, 818 ppm Ru, 126 ppm Ir, 81 ppm Os), while tenors of semi-massive to massive sulfides are lower but more consistent (<2 ppm Pt and Os, <3 ppm Pd, <4 ppm Ir, <12 ppm Rh and <18 ppm Ru).
3. An almost exclusively Ir-As, IPGE+Pt-As-S and Ru-S PGM assemblage, with minor Ir-alloys, PPGE-As, Pt±Pd-Bi-Te, Pt-Fe and Au-Ag.
4. Palladium hosted almost exclusively within pentlandite and Pt hosted almost exclusively by PGM, while IPGE+Rh are hosted variably by PGM and sulfides, apparently correlating with the volume of sulfide in the sample.

Processes controlling the formation of IPGE+Rh dominant mineralization

The most significant finding of this study is the dominance of IPGE+Rh compared to Pt+Pd+Au within the BM Zone—a highly unusual feature for a magmatic sulfide deposit. High IPGE+Rh contents within magmatic sulfide deposits can occur through, and are related to several different processes, including (1) chromite formation, (2) fractionation of sulfide melt, or (3)

involvement of late-magmatic or hydrothermal fluids. Within the Bushveld Complex, the most well-known PGE horizons to show high (IPGE+Rh)/(Pt+Pd) ratios are the Lower Critical Zone hosted LG-1 to LG-4 chromitites (Naldrett et al., 2009). These are “chromitite-controlled” horizons with very low sulfide content, meaning PGE was predominately concentrated by chromite, rather than a sulfide liquid. This results in a characteristic IPGE+Rh enrichment relative to Pt+Pd+Au (Scoon and Teigler, 1994). However, this process does not explain the IPGE+Rh-dominance at Sandsloot, as the BM Zone lacks significant chromite. No chromitites or chromite seams have been noted and whole-rock geochemistry shows very low Cr_2O_3 values (Fig. 6). Furthermore, PGE mineralization is clearly sulfide-associated (Fig. 11a).

Alternatively, late-magmatic or hydrothermal fluids may have played a role in separating IPGE+Rh from Pt+Pd+Au. Within the Northern Limb, fluid activity has been shown to be an important control on mobilising some metals (e.g., Armitage et al., 2002; Holwell et al., 2006, 2017; Smith et al., 2014). Evidence of fluid involvement in the BM Zone at Sandsloot includes skarn textures (Fig. 4f), chlorite and serpentinite alteration, and carbonate veinlets (Fig. 5e-g). Platinum-group minerals are also stranded in sulfide alteration halos in places (Fig. 11a, h). Under typical hydrothermal conditions, such as serpentinisation and talc-carbonate alteration, Cu and Au are extremely mobile, Pd and Ni are moderately mobile, while Pt, Rh and IPGE are far less mobile (Barnes and Liu, 2012). As such, hydrothermal mobilisation can fractionate Cu, Au, and Pd from Rh and the IPGE quite effectively. The BM Zone ores have Pt/Pd ratios generally <1 (average 0.7; Fig. 7b), which are typical of most Northern Limb PGE deposits (McDonald et al., 2005). If PGE had been mobilised away from the BM Zone, Pd would be expected to be lower than Pt due to its higher mobility. Furthermore, there are no systematic changes in other immobile/mobile element ratios, such as Rh/Pd, between the least and most heavily altered samples (Table. 2). However, it is possible under highly oxidised, acidic conditions to also mobilise Pt and Ni (Barnes and Liu, 2012; Liu et al., 2012). Alternatively, more reduced fluids can mobilise Pt if there is high salinity (Sullivan et al., 2022). Where this alteration has occurred in other areas of the Northern Limb, significant volumes of pyrrhotite

are lost, sulfides are replaced by secondary pyrite and millerite, and IPGE+Rh are typically hosted by secondary pyrite (e.g., Grasvally Norite-Pyroxenite-Anorthosite member; Holwell et al., 2017). This style of mineralization is distinctly to anything seen within the BM Zone. Therefore, an alternative explanation for the IPGE-rich nature of the BM Zone is required.

Sulfide liquid fractionation can be an extremely effective mechanism to physically separate Fe-Ni-Rh-IPGE monosulfide solid solution (MSS) from Cu-Au-Pt-Pd intermediate solid solution (ISS). The primitive mantle-normalized PGE plots (Fig. 8a) of both the disseminated/blebby and semi-massive/massive sulfides display a pattern which is similar to those from Fe-sulfide rich ores, such as at the Creighton Ni-Cu-PGE deposit, Sudbury and Western Jinchuan Intrusion, NW China (Dare et al., 2010a; Chen et al., 2013). In these deposits the IPGE-rich profiles are thought to represent the Fe-rich MSS portion of a cooled and fractionated sulfide liquid, which is associated with the process of partitioning of Os, Ir, Ru and Rh into MSS, while Pt, Pd and Au go into residual the Cu-rich liquid. Upon further cooling this Cu-rich liquid forms ISS (Li et al., 1996; Barnes et al., 1997). This provides an effective mechanism to produce the IPGE+Rh-dominant sulfide in the BM Zone. However, if the BM Zone is representative of the MSS portion of a sulfide liquid, this leaves a mass balance problem. Specifically, to explain the concentrations of Ni-IPGE+Rh observed there must be significant Cu-Pt+Pd+Au elsewhere.

It is known that between 900°C and 800°C MSS crystallizes, separating a residual Cu-rich liquid (Kitakaze and Sugaki, 2004; Kitakaze et al., 2016). This residual liquid has the potential to migrate away from MSS on a variety of scales (e.g., Blanks et al., 2022). In the BM Zone, this process is observed on a mm to cm scale, where chalcopyrite has migrated to the boundaries of the symplectite semi-massive sulfides and into the surrounding silicates (Fig. 4c), as well as through fractionated sulfide veins (Fig. 4d, 5f-g). However, this phenomenon can occur on a much larger deposit-wide scale. Multiple examples of deposit scale separation of a Cu(+Pt+Pd+Au)-rich liquid from Fe-rich MSS exist. These include the Jinchuan Intrusion, NW China (Chen et al., 2013); the McCreedy East (Dare et al., 2014) and Rathbun deposits

(Kawohl et al., 2020), Sudbury Igneous Complex, Canada; the Munali Ni-Cu-PGE deposit, Zambia (Blanks et al., 2022); and the Sakatti Cu-Ni-PGE deposit, N Finland (Brownscombe et al., 2015). Although no Cu-rich sections have yet been identified in the BM Zone, it is intriguing that samples from the very base of the BM Zone are more Cu-rich and exhibit a more positive primitive mantle-normalized PGE profile (Fig. 8a). This suggests a higher proportion of ISS relative to MSS, differing from the rest of the BM Zone. This profile is similar to those from intermediately fractionated sulfides that occur at the Eagle Ni-Cu deposit, United States (Ding et al., 2012). Further support for this interpretation is provided by Rh/Cu ratios plotted downhole. Since Rh is highly compatible within MSS, while Cu is highly incompatible in MSS (and conversely highly compatible in ISS), Rh/Cu ratios can be used to establish the degree of fractionation of a sulfide liquid as essentially a proxy for MSS/ISS (Naldrett et al., 1999; Naldrett et al., 2000). The Rh/Cu ratio decreases with depth through SA19, with the lowest Rh/Cu ratios observed in the samples from the deepest intersection (Fig. 13). The presence of intermediately fractionated PGE profiles towards the base of the BM Zone suggests that Cu-rich residual liquids, enriched in the missing Pt, Pd and Au, were mobilized further downwards. To date footwall rocks have not been intersected to the deep Platreef at Sandsloot; thus, an undiscovered Cu-Pt-Pd-rich zone at depth or down-dip remains a possibility.

The steepness of the negative PGE slope from Rh through Au in the BM Zone at Sandsloot (Fig. 8a) is significantly more extreme than any of the other IPGE-dominant deposits (e.g., Creighton Ni-Cu-PGE deposit, Sudbury and Western Jinchuan Intrusion, NW China; Dare et al., 2010b; Chen et al., 2013). This indicates there may be an additional control on the extreme enrichment of IPGE+Rh relative to Pt+Pd+Au. While sulfide liquid fractionation can effectively separate Cu and Ni sulfide it is important to note that the Cu-rich veins and zones, where it appears Cu-sulfide has migrated, are associated with calcite (Fig. 3e, 5e-g). An association between carbonate and sulfide, including Cu-rich sulfides has been noted in several Ni-Cu-PGE deposits (e.g., Blanks et al., 2022; Cherdantseva et al., 2023). Thompson et al. (2025a)

and Thompson et al. (*in review*) describe the BM Zone as a skarn-like system, based on geochemical signatures from major elements. Therefore, given the close association of calcite with Cu-sulfide, it raises the possibility that some of the missing Pt+Pd+Au may have been mobilised from the orebody by metasomatic fluids, rather than, or in addition to, a pure sulfide fractionation process. Thompson et al. (*in review*) show the silicate mineralogy in the BM Zone to be skarn-like, with pegmatoidal textures, high prehnite volumes (Fig. 4c, f), and high An contents in plagioclase; alongside Niggli numbers that trend towards skarn assemblages (Thompson et al., 2025a).

It is notable, however, that sulfide veins, which show a separation of Cu and Ni (Fig. 4d) and can be associated with carbonate (Fig. 5d, e), contain comparable Pd contents in pentlandite to the disseminated/blebby or semi-massive/massive sulfides with which they are spatially associated. If Pd (alongside Cu+Pt+Au) had been lost from the BM Zone through metasomatic fluid interaction, it would be expected that Pd contents of pentlandite should vary between vein sulfides and the other sulfide textures. Furthermore, an abundance of low temperature PGM species should be present if fluids mobilised Pt+Pd+Au, which are not recorded. Therefore, while skarn-like processes appear to have affected the silicate mineralogy, we do not consider this process to be the main driver for the Cu+Pt+Pd-Au-poor nature of the BM Zone and consider the separation of Cu and Ni sulfide to be a magmatic feature related to fractional crystallisation of a sulfide liquid.

Processes controlling sulfide tenor variations

There is a clear difference in the PGE tenors between the semi-massive/massive sulfides and the disseminated/blebby sulfides (Table 3, Fig. 14a). A number of different factors can influence PGE tenors, such as different degrees of fractionation, R-factor (the ratio of sulfide liquid to silicate magma), fluid involvement and the addition of crustal S (Queffurus and Barnes, 2015).

Under low temperature hydrothermal conditions (<300 °C) S is typically far more mobile than PGE. This means hydrothermal alteration can act to increase sulfide tenors by removing S,

reducing the volume of sulfide without removing the PGE and leading to PGE enrichment (Queffurus and Barnes, 2015; Smith et al., 2016). Although there is minor alteration of sulfide around their boundaries in the BM Zone (Fig. 4c), tenors should vary dependent upon the degree of alteration if hydrothermal activity were responsible. However, tenors do not show this variation. Instead, they vary depending upon whether sulfides are semi-massive/massive or disseminated/blebby. This suggests that either variable R-factors or involvement of crustal S are more likely controls.

In zones of semi-massive/massive sulfides, where large amounts of sulfide have accumulated, the sulfide liquid is present with a low ratio of sulfide liquid to silicate magma. As a result, R-factors and metal tenors would be lower compared to the rest of the BM Zone, where droplets may have equilibrated with a greater volume of magma (thus producing higher R-factors). Variations in R-factor also have an influence on Se contents, meaning S/Se ratios should decrease with increasing R factor. Therefore, the highest tenor sulfides should have the lowest S/Se ratios (Thériault et al., 1997). The S/Se ratios are higher (average = 7536) within semi-massive/massive sulfides than disseminated/blebby sulfides (average = 4390), providing support of the differences in sulfide tenors being an R-factor effect.

An alternative explanation to R-factor being the key control on sulfide tenors is the addition of crustal S. The initial sulfide liquid may have been very high tenor, but locally crustal S was assimilated, essentially diluting the sulfides to lower tenors. This process would also increase the S/Se ratios. Therefore, the observed differences in S/Se ratios and PGE tenors between the different sulfide styles can alternatively be explained through this process. The disseminated/blebby sulfides represent an initial high-tenor sulfide liquid, while semi-massive/massive sulfides represent high-tenor sulfides diluted by crustal S. Given that the Malmani Subgroup dolomite, a likely source of crustal S (Buchanan et al., 1981; Buchanan and Rouse, 1984), forms the footwall of the shallow Platreef at Sandsloot we favour this mechanism over differences in R-factor. Support of this is provided by Thompson et al. (2025a) and Thompson et al. (*in review*) who describe the extensive interaction of the BM

Zone with the Malmani Subgroup sediments, which are known to contain S-bearing anhydrite layers (Buchanan and Rouse, 1984).

Whilst the IPGE sulfide tenors in the BM Zone are unusually high, very high sulfide tenors (up to 45 ppm Os, 147 ppm Ir, 506 ppm Ru, 296 ppm Rh, 1239 ppm Pt, 683 ppm Pd) have also been reported by Holwell et al. (2006) and Jones (2013) from chromite-hosted homogenized sulfide inclusions in the shallow Platreef. As these inclusions are trapped within the earliest crystallizing phase, chromite, they are believed to represent an early high tenor parental sulfide liquid to the Platreef. In Figure 14, the PGE tenors of the chromite-hosted inclusions are compared to those of the BM Zone. The chromite-hosted inclusions are divided into Ni-rich, which essentially represent an MSS-dominant portion of the sulfide liquid, Cu-rich, which represent an ISS-dominant portion of the sulfide liquid, and inclusions which are mixtures of both MSS and ISS. As expected, the BM Zone has chondrite-normalized PGE profiles which are most similar to the Ni-rich homogenized inclusions, although the depletion in Pt+Pd+Au is far more extreme in the BM Zone. However, what is most striking is the BM Zone has IPGE tenors that overlap with (in the case of massive/semi-massive sulfides) or are higher (in the case of disseminated/blebby sulfides) than the chromite-hosted sulfide inclusions (Fig. 14). Since the BM Zone represents only the MSS portion of the sulfide liquid, if the Pt+Pd+Au tenors were to be extrapolated to also include the ISS portion of the sulfide liquid (i.e. the parental sulfide liquid) the Pt+Pd+Au tenors would overlap with, or indeed exceed, those of the chromite-hosted sulfide inclusions presented by Holwell et al. (2011) and Jones (2013).

This finding has broader implications for the genesis of Platreef mineralization. Several authors have suggested that the initial sulfide liquid of the Platreef was already highly enriched in PGE prior to emplacement (e.g., McDonald and Holwell, 2007; Holwell et al., 2011), with crustal S diluting tenors on a localised scale (e.g., Sharman-Harris et al., 2005; Holwell et al., 2007; Ihlenfeld and Keays, 2011). Others (e.g., Buchanan and Rouse, 1984; Grobler et al., 2019; Maier et al., 2021; 2023) have proposed the sulfide liquid was upgraded to high tenors during magma emplacement. The IPGE tenors within the BM Zone are higher than any

elsewhere in the Platreef and are comparable to the very high tenor chromite-hosted sulfide inclusions reported by Holwell et al. (2011) and Jones (2013), which are thought to represent a trapped early high tenor parental sulfide liquid. Thus, this could support the idea that the BM Zone is representative of (at least an MSS portion of) that initial, high tenor sulfide liquid. The location of the BM Zone down-dip and west of the shallow Platreef is perhaps intriguing in this regard, as it has been proposed previously by McDonald et al. (2009) and Yudovskaya et al. (2011) that a high-grade feeder zone may be located down-dip and west of the shallow Platreef at Sandsloot.

To generate such high PGE tenors prior to emplacement, a staging chamber model has been proposed (e.g., McDonald and Holwell, 2007; McDonald et al., 2009). In this model sulfide droplets are formed and enriched with metals in a high R factor environment within a deep-seated staging chamber prior to magma emplacement. These sulfides are then entrained during Platreef magma ascent (Holwell et al., 2007; Smith et al., 2016). Based upon the comparable tenors of the chromite-hosted sulfide inclusions and BM Zone sulfides we favour this model of PGE enrichment.

Sulfide and PGM crystallisation history

Figure 15 presents a schematic representation of the crystallization history and PGE behaviour as the BM Zone formed and cooled. Within a S-rich, alloy poor system such as the BM Zone, IPGE+Rh are highly compatible within MSS. Therefore, they are usually contained within pentlandite and pyrrhotite (Fleet et al., 1993; Li et al., 1996; Barnes et al., 1997; Mungall et al., 2005; Mansur et al., 2021). However, in the BM Zone the proportion of IPGE contained within sulfide is variable (Fig. 9b-e), with significant IPGE also contained within PGM arsenide, arsenosulfides and sulfide phases (Fig. 10, 11), such as Os+Ir-bearing laurite, irasite and iridarsenite. Through experimental studies Helmy and Bragagni (2017) demonstrated that the formation of IPGE+Pt sulfoarsenides is highly dependent upon the activity of As within a system, which in turn is strongly controlled by S fugacity (fS_2). When fS_2 is lowest, around 1100 °C, As is moderately compatible within the early crystallising MSS (Helmy et al., 2010;

Helmy et al., 2013; Helmy and Bragagni, 2017; Piña et al., 2020). As a result, IPGE+Pt can form early, high temperature PGE-sulfoarsenides directly from the sulfide melt (Dare et al., 2010a; Chashchin et al., 2021). The often euhedral, sulfide-hosted nature of the PGE-sulfoarsenides in the BM Zone (e.g., Fig. 11) is consistent with their formation before crystallisation of MSS (Liang et al., 2019). At these high temperatures, the strong affinity of As to complex Ir and Pt promotes crystallisation of Ir and Pt- arsenosulfides, whilst Os and Ru have a stronger affinity for S than As, forming Ru(Os)-sulfides (Fig. 15e1; Helmy and Bragagni, 2017). This is entirely consistent with the PGM mineralogy we observe at Sandsloot (Fig. 10, 11), and we therefore propose that most of the IPGE-PGM formed in this way (Fig. 15e1). High temperature Ir, Pt, Ru±Os PGM have also been described in the Creighton Ni-Cu-PGE deposit, hosted within early MSS cumulates (Dare et al., 2010a), analogous to those we describe at Sandsloot. Our mass balance highlights only up to 64% of the Rh is accounted for in sulfide. However, few Rh-bearing PGM were identified in the PGM analysis, suggesting Rh PGM may have been missed from the PGM analysis due to nugget effects. Given the abundance of irasite and platarsite, any missing Rh PGM may be present in the form of hollingworthite, which belongs to the same solid solution series.

Unlike IPGE+Pt, Pd does not form high-temperature semi-metal complexes with As or S (Helmy et al., 2010; Helmy et al., 2013; Helmy and Bragagni, 2017) and, therefore, will have stayed within the sulfide liquid after the formation of high temperature Os-Ir-Ru-Rh-Pt PGM. The IPGE+Rh, as well as Co, are highly compatible within MSS, so any IPGE+Rh which did not form the early arsenosulfide PGM, along with Co, entered MSS (Li et al., 1996; Barnes et al., 1997; Mungall et al., 2005; Mansur et al., 2021). Monosulfide solid solution subsequently crystallizes pentlandite and pyrrhotite at lower temperatures; however, pentlandite formation can also occur at high temperatures (Kitakaze et al., 2016). Several authors (e.g., Dare et al., 2010a; Mansur et al., 2019; Barnes et al., 2020) have highlighted that pentlandite textures can provide insight into the crystallization history of sulfide liquids. Within the massive/semi-massive sulfides, loop-textured pentlandite around pyrrhotite (Fig. 4c) and contact pentlandite

between chalcopyrite and pyrrhotite (Fig. 4b) are present. Whereas, within disseminated/blebby sulfides, granular pentlandite occurs around pyrrhotite boundaries (Fig. 5a. b). Work by Barnes et al. (2020) and Mansur et al. (2019) shows that these pentlandite textures are products of high-temperature peritectic reaction. Kitakaze et al. (2016) experimentally demonstrated that this reaction occurs between 870° and 740°C, between early crystallized MSS and residual Pd-rich sulfide liquid and producing Pd-rich pentlandite. In contrast, lower-temperature exsolution pentlandite is typically Pd-poor (e.g., Barnes et al. 2020). The findings that almost 100% of Pd is contained within pentlandite (Fig. 12), that Pd contents of pentlandite can be high (Fig. 9a) and the presence of peritectic sulfide textures (Fig. 4b, c) are all consistent with formation of pentlandite at high temperatures that incorporated Pd, as well IPGE+Rh+Co (Fig. 15e3).

Conversely to IPGE+Rh, Pt+Pd+(Au+Ag+Bi+Te) are highly incompatible within MSS, as well as ISS (Dare et al., 2014; Liu and Brenan, 2015; Mansur et al., 2020; Mansur et al., 2021). Therefore, Pt+(Au+Ag+Bi+Te), alongside any Pd not incorporated by high temperature pentlandite, were concentrated into a semi-metal rich residual liquid (e.g., Helmy et al., 2010; Liu and Brenan, 2015; Mansur et al., 2020). This liquid would have crystallized Pt±Pd-Bi-Te PGM and Au-Ag below 650°C (Fig. 15e4). However, the relative concentrations of semimetal to Pd were low, as Pd was almost entirely taken up by high temperature pentlandite rather than remaining in the residual sulfide liquid (Holwell and McDonald, 2010). Below 650 °C (Kelly and Vaughan, 1983) pyrrhotite and pentlandite crystallised from MSS. Both phases subsequently trapped IPGE and Co. Minor exsolution of pentlandite from MSS produced the flames-textured pentlandite in pyrrhotite observed (Fig. 4b. Fig. 15e4). As discussed above, Cu-rich sulfide liquid may have separated from the main MSS mass preserved in the BM Zone. It likely migrated down-dip, or into the footwall rocks (Fig. 15e2), crystallising first ISS and then chalcopyrite (Kelly and Vaughan, 1983).

Comparison of the BM Zone to sulfide-rich intersections in the wider Platreef

Throughout the Northern Limb, massive sulfides are sporadically developed towards the base of the shallow Platreef. These have been attributed to downward percolation and ponding of Platreef sulfide based on their distribution in structural traps (e.g., Turfspruit and Macalaskop Hutchinson and Kinnaird 2005; Tweefontein Hill, Nex 2005). Thompson et al. (2025a) and Thompson et al. (*in review*) suggest that the BM Zone in the deep Platreef at Sandsloot formed in a similar manner, through slumping and accumulation of sulfide towards the Platreef's base. In Figure 8 primitive mantle-normalized PGE profiles of the BM Zone are compared to net-textured and semi-massive sulfides present at the base of the shallow Platreef at Tweefontein Hill (Fig. 1). The PGE profiles of the Tweefontein Hill semi-massive sulfides is more akin to that of typical Platreef than the BM Zone; i.e., not MSS-like. Additionally, the PGM assemblage at Tweefontein Hill is dominated by Pt-Pd-Bi-Te (Martin, 2018), rather than any IPGE-rich PGM as seen in the BM Zone. As suggested previously by Nex (2005), the PGE profiles and PGM assemblages support that the Tweefontein Hill semi-massive sulfides represent accumulations of Platreef sulfide. Other reported occurrences of massive sulfides at the base of the shallow Platreef (e.g., Turfspruit and Macalacaskop; Hutchinson and Kinnaird, 2005) are characterized by significant proportions of chalcopyrite, and as such do not represent MSS. Therefore, while the BM Zone shares a similar stratigraphic location to other occurrences of semi-massive/massive sulfides in the Platreef, there are clear geochemical and mineralogical differences.

While IPGE+Rh-rich ores have not been reported in other occurrences of sulfide-rich ores in the Bushveld, Ir-Rh-Ru-rich PGM have been noted in the deep Platreef at Akanani, down-dip from the Zwartfontein pit (Fig. 1a). It is thought these PGM represent an early assemblage that crystallised at high temperatures; however, this assemblage is found in harzburgites which are much poorer in sulfide than the BM Zone. Additionally, despite the abundance of Ir-Rh-Ru-rich PGM, mineralization is still Pt-Pd dominant rather than IPGE-Rh dominant (Yudovskaya et al., 2011). This makes it distinct from the Sandsloot BM Zone.

What is apparent from the aforementioned comparisons is the BM Zone is not simply the MSS portion of the sulfide liquid from the overlying PGE-Reef, and appears to be a distinct sulfide generation. Additionally, the BM Zone appears to become more fractionated with depth, suggesting if an ISS portion was to exist this should be beneath the BM Zone rather than above where the PGE-Reef is located. This leaves three possibilities, either (1) the BM Zone is unrelated to the PGE-Reef, (2) the BM Zone is an accumulation of the same sulfide found in the PGE-Reef, but this sulfide has only undergone fractionation in the BM Zone or (3) the BM Zone is part of the same system as the PGE-Reef, but represents an earlier (fractionated) high tenor sulfide liquid.

Thompson et al. (*in review*) do not distinguish the BM Zone and PGE-Reef in the Sandsloot deep Platreef (Fig. 1b) as distinct magmatic pulses, as they have similar geochemical signatures. However, this study shows that the sulfides and associated PGE in the PGE Reef and the BM zone do not appear to be genetically related. Therefore, it is possible that the sequence may have been made up of chemically similar pulses of magma, but preserve two distinct generations of sulfide.

Conclusions

The BM Zone, located in the deep Platreef at Sandsloot, represents a new style of mineralization in the context of the Northern Limb. It is distinct from other sulfide-enriched portions along the base of the Platreef, as it has very high (Os+Ir+Rh+Ru)/(Pt+Pd) ratios, being an IPGE+Rh-dominant zone opposed to Pt+Pd. The BM Zone is Fe-sulfide rich and contains predominately pyrrhotite-dominant magmatic sulfides, with lesser pentlandite and chalcopyrite. It has a PGM assemblage dominated by IPGE+Pt-arsenosulfides, which are typically closely associated with sulfide. Pentlandite and pyrrhotite also host IPGE+Rh, whilst Pd is almost exclusively hosted by pentlandite.

We propose the BM Zone represents the MSS portion of a sulfide liquid body, resulting in very high IPGE contents and high (IPGE+Rh)/(Pt+Pd) and Ni/Cu ratios. The sulfide liquid

fractionated downwards through the BM Zone, producing intermediately fractionated sulfides, with lower (Os+Ir+Rh+Ru)/(Pt+Pd) ratios towards the base of the BM Zone (Fig. 15b). The Cu+Pt+Pd+Au-poor nature of the BM Zone is the result of migration of Cu-rich sulfide liquids away from MSS during solidification of the melt (Fig. 15c). Dilution of tenors by addition of crustal S, or variable R-factor regimes, is responsible for the tenor variations between low-PGE tenor massive/semi-massive sulfides and high-PGE tenor disseminated/blebby sulfides (Fig. 15d).

Further understanding of the fractionation trend throughout the BM Zone may benefit future exploration, as the BM Zone represents an MSS portion of the parental sulfide liquid which fractionated downwards. This suggests a Cu-rich portion, with associated Pt+Pd+Au, may be present at greater depths, not yet intersected by drilling. Alternatively, the Cu-rich residual liquid was mobilised away from Sandsloot.

Acknowledgments

This research was funded by Anglo American through the Northern Limb in 4D (NL4D) consortium, awarded to the University of Leicester, Cardiff University and University of Exeter. The Society of Economic Geologists (SEG) provided additional funding for geochemical and SEM analysis through the SEG Foundation Student Research Grant SRG 23-84. We also acknowledge Anglo American for logistical support with fieldwork and providing access to drillcores for sampling and downhole assay data. Additionally, Lin Marvin is thanked for assistance with XRF analysis, Annika Burns for preparation of thin sections, Adam Cox for assistance with LA-ICP-MS analysis and Leon Hicks for assistance with SEM analysis. We are grateful for the reviews of M.C. Jenkins and an anonymous reviewer, and editorial handling by Dave Cooke, who helped to improve the quality and focus of the manuscript.

References

Armitage, P.E.B., McDonald, I., Edwards, S.J., and Manby, G.M., 2002, Platinum-group element mineralization in the Platreef and calc-silicate footwall at Sandsloot, Potgietersrus District, South Africa: Applied Earth Science, v. 111, no. 1, p. 36–45.

Ashwal, L.D., Webb, S.J., and Knoper, M.W., 2005, Magmatic stratigraphy in the Bushveld Northern Lobe: continuous geophysical and mineralogical data from the 2950 m Bellevue drillcore: South African Journal of Geology, v. 108, no. 2, p. 199–232.

Barnes, S.-J., and Lightfoot, P.C., 2005, Formation of magmatic nickel-sulfide ore deposits and processses affecting their copper and platinum-group element contents, *in* Hedenquist, J.W., Thompson, J.F.H., Goldfarb, R.J., and Richards, J.P. eds., Economic Geology 100th Anniversary: Littleton, CO, Society of Economic Geologist, p. 179–213.

Barnes, S.J., and Liu, W., 2012, Pt and Pd mobility in hydrothermal fluids: Evidence from komatiites and from thermodynamic modelling: Ore Geology Reviews, v. 44, p. 49–58.

Barnes, S.-J., Makovicky, E., Makovicky, M., Rose-Hansen, J., and Karup-Moller, S., 1997, Partition coefficients for Ni, Cu, Pd, Pt, Rh, and Ir between monosulfide solid solution and sulfide liquid and the formation of compositionally zoned Ni – Cu sulfide bodies by fractional crystallization of sulfide liquid: Canadian Journal of Earth Sciences, v. 34, no. 4, p. 366–374.

Barnes, S.J., Taranovic, V., Schoneveld, L.E., Mansur, E.T., Le Vaillant, M., Dare, S., Staude, S., Evans, N.J., and Blanks, D., 2020, The Occurrence and Origin of Pentlandite-Chalcopyrite-Pyrrhotite Loop Textures in Magmatic Ni-Cu Sulfide Ores: Economic Geology, v. 115, no. 8, p. 1777–1798.

Blanks, D.E., Holwell, D.A., Barnes, S.J., Schoneveld, L.E., Fiorentini, M.L., Baublys, K.A., Mbiri, L., and Knott, T.R., 2022, Mobilization and Fractionation of Magmatic Sulfide: Emplacement and Deformation of the Munali Ni-(Cu-Platinum Group Element) Deposit, Zambia: Economic Geology, v. 117, no. 8, p. 1709–1729.

Brownscombe, W., Ihlenfeld, C., Coppard, J., Hartshorne, C., Klatt, S., Siikaluoma, J.K., and Herrington, R.J., 2015, The Sakatti Cu-Ni-PGE Sulfide Deposit in Northern Finland, *in* Maier, W.D., Lahtinen, R., and O'Brien, H. eds., Mineral Deposits of Finland: Elsevier, p. 211–252.

Buchanan, D.L., and Rouse, J.E., 1984, Role of contamination in the precipitation of sulphides in the Platreef of the Bushveld complex, *in* Buchanan, D.L. and Jones, J.M. eds., Sulfide deposits in mafic and ultramafic rocks: London, Institution of Mining and Metallurgy, p. 141–146.

Buchanan, D.L., Nolan, J., Suddaby, P., Rouse, J.E., Viljoen, M.J., and Davenport, J.W.J., 1981, The genesis of sulfide mineralization in a portion of the Potgietersrus Limb of the Bushveld Complex: Economic Geology, v. 76, no. 3, p. 568–579.

Cawthorn, R.G., 1999, Platinum-group element mineralization in the Bushveld Complex–a critical reassessment of geochemical models.: South African Journal of Geology, p. 102.

Chashchin, V.V., Petrov, S.V., Kiseleva, D.V., and Savchenko, Ye.E., 2021, Platinum Content and Formation Conditions of the Sulfide PGE–Cu–Ni Nyud-II Deposit of the Monchegorsk Pluton, Kola Peninsula, Russia: Geology of Ore Deposits, v. 63, no. 2, p. 87–117.

Chen, L.-M., Song, X.-Y., Keays, R.R., Tian, Y.-L., Wang, Y.-S., Deng, Y.-F., and Xiao, J.-F., 2013, Segregation and Fractionation of Magmatic Ni-Cu-PGE Sulfides in the Western

Jinchuan Intrusion, Northwestern China: Insights from Platinum Group Element Geochemistry: Economic Geology, v. 108, no. 8, p. 1793–1811.

Cherdantseva, M., Vishnevskiy, A., Jugo, P.J., Martin, L.A.J., Aleshin, M., Roberts, M.P., Shaparenko, E., Langendam, A., Howard, D.L., and Fiorentini, M.L., 2023, Caught in the moment: interaction of immiscible carbonate and sulfide liquids in mafic silicate magma—insights from the Rudniy intrusion (NW Mongolia): Mineralium Deposita, v. 59, p. 733-755.

Dare, S.A.S., Barnes, S.-J., Prichard, H.M., and Fisher, P.C., 2010a, The Timing and Formation of Platinum-Group Minerals from the Creighton Ni-Cu-Platinum-Group Element Sulfide Deposit, Sudbury, Canada: Early Crystallization of PGE-Rich Sulfarsenides: Economic Geology, v. 105, no. 6, p. 1071–1096.

Dare, S.A.S., Barnes, S.-J., and Prichard, H.M., 2010b, The distribution of platinum group elements (PGE) and other chalcophile elements among sulfides from the Creighton Ni–Cu–PGE sulfide deposit, Sudbury, Canada, and the origin of palladium in pentlandite: Mineralium Deposita, v. 45, no. 8, p. 765–793.

Dare, S.A.S., Barnes, S.-J., Prichard, H.M., and Fisher, P.C., 2014, Mineralogy and Geochemistry of Cu-Rich Ores from the McCreedy East Ni-Cu-PGE Deposit (Sudbury, Canada): Implications for the Behavior of Platinum Group and Chalcophile Elements at the End of Crystallization of a Sulfide Liquid: Economic Geology, v. 109, no. 2, p. 343–366.

Ding, X., Ripley, E.M., and Li, C., 2012, PGE geochemistry of the Eagle Ni–Cu–(PGE) deposit, Upper Michigan: constraints on ore genesis in a dynamic magma conduit: Mineralium Deposita, v. 47, no. 1, p. 89–104.

Fischer-Gödde, M., Becker, H., and Wombacher, F., 2010, Rhodium, gold and other highly siderophile element abundances in chondritic meteorites: Geochimica et Cosmochimica Acta, v. 74, no. 1, p. 356–379.

Fleet, M.E., Chryssoulis, S.L., Stone, W.E., and Weisener, C.G., 1993, Partitioning of platinum-group elements and Au in the Fe−Ni−Cu−S system: experiments on the fractional crystallization of sulfide melt: Contributions to Mineralogy and Petrology, v. 115, no. 1, p. 36–44.

Godel, B., Barnes, S.-J., and Maier, W.D., 2007, Platinum-Group Elements in Sulphide Minerals, Platinum-Group Minerals, and Whole-Rocks of the Merensky Reef (Bushveld Complex, South Africa): Implications for the Formation of the Reef: Journal of Petrology, v. 48, no. 8, p. 1569–1604.

Grobler, D.F., Brits, J.A.N., Maier, W.D., and Crossingham, A., 2019, Litho- and chemostratigraphy of the Flatreef PGE deposit, northern Bushveld Complex: Mineralium Deposita, v. 54, no. 1, p. 3–28.

Hall, A., 1932, The Bushveld Igneous Complex in the central Transvaal: Geological Survey of South Africa Memoir 28, 560 p.

Harris, C., and Chaumba, J.B., 2001, Crustal Contamination and Fluid–Rock Interaction during the Formation of the Platreef, Northern Limb of the Bushveld Complex, South Africa: Journal of Petrology, v. 42, no. 7, p. 1321–1347.

Helmy, H.M., and Bragagni, A., 2017, Platinum-group elements fractionation by selective complexing, the Os, Ir, Ru, Rh-arsenide-sulfide systems above 1020 °C: Geochimica et Cosmochimica Acta, v. 216, p. 169–183.

Helmy, H.M., Ballhaus, C., Wohlgemuth-Ueberwasser, C., Fonseca, R.O.C., and Laurenz, V., 2010, Partitioning of Se, As, Sb, Te and Bi between monosulfide solid solution and sulfide melt – Application to magmatic sulfide deposits: Geochimica et Cosmochimica Acta, v. 74, no. 21, p. 6174–6179.

Helmy, H.M., Ballhaus, C., Fonseca, R.O.C., and Nagel, T.J., 2013, Fractionation of platinum, palladium, nickel, and copper in sulfide–arsenide systems at magmatic temperature: Contributions to Mineralogy and Petrology, v. 166, no. 6, p. 1725–1737.

Holwell, D.A., and McDonald, I., 2006, Petrology, geochemistry and the mechanisms determining the distribution of platinum-group element and base metal sulphide mineralisation in the Platreef at Overysel, northern Bushveld Complex, South Africa: Mineralium Deposita, v. 41, p. 575–598.

Holwell, D.A., and McDonald, I., 2007, Distribution of platinum-group elements in the Platreef at Overysel, northern Bushveld Complex: a combined PGM and LA-ICP-MS study: Contributions to Mineralogy and Petrology, v. 154, no. 2, p. 171–190.

Holwell, D.A., and McDonald, I., 2010, A Review of the Behaviour of Platinum Group Elements within Natural Magmatic Sulfide Ore Systems: Platinum Metals Review, v. 54, p. 26–36.

Holwell, D.A., McDonald, I., and Armitage, P.E.B., 2006, Platinum-group mineral assemblages in the Platreef at the Sandsloot Mine, northern Bushveld Complex, South Africa: Mineralogical Magazine, v. 70, no. 1, p. 83–101.

Holwell, D.A., Boyce, A.J., and McDonald, I., 2007, Sulfur Isotope Variations within the Platreef Ni-Cu-PGE Deposit: Genetic Implications for the Origin of Sulfide Mineralization: Economic Geology, v. 102, no. 6, p. 1091–1110.

Holwell, D.A., McDonald, I., and Butler, I.B., 2011, Precious metal enrichment in the Platreef, Bushveld Complex, South Africa: evidence from homogenized magmatic sulfide melt inclusions: Contributions to Mineralogy and Petrology, v. 161, no. 6, p. 1011–1026.

Holwell, D.A., Adeyemi, Z., Ward, L.A., Smith, D.J., Graham, S.D., McDonald, I., and Smith, J.W., 2017, Low temperature alteration of magmatic Ni-Cu-PGE sulfides as a source for hydrothermal Ni and PGE ores: A quantitative approach using automated mineralogy: Ore Geology Reviews, v. 91, p. 718–740.

Hutchinson, D., and Kinnaird, J.A., 2005, Complex multistage genesis for the Ni–Cu–PGE mineralisation in the southern region of the Platreef, Bushveld Complex, South Africa: Applied Earth Science, v. 114, p. 208–224.

Ihlenfeld, C., and Keays, R.R., 2011, Crustal contamination and PGE mineralization in the Platreef, Bushveld Complex, South Africa: evidence for multiple contamination events and transport of magmatic sulfides: Mineralium Deposita, v. 46, no. 7, p. 813–832.

Jones, R.E., 2013, Petrological and geochemical study of Platreef chromitites, northern Bushveld, South Africa: Ph.D. thesis, Cardiff, Cardiff University, 280 p.

Kawohl, A., Whymark, W.E., Bite, A., and Frimmel, H.E., 2020, High-Grade Magmatic Platinum Group Element-Cu(-Ni) Sulfide Mineralization Associated with the Rathbun Offset Dike of the Sudbury Igneous Complex (Ontario, Canada): Economic Geology, v. 115, no. 3, p. 505–525.

Kelly, D.P., and Vaughan, D.J., 1983, Pyrrhotine-pentlandite ore textures: a mechanistic approach: Mineralogical Magazine, v. 47, p. 453–463.

Kinnaird, J.A., and McDonald, I., 2018, The northern limb of the Bushveld Complex: a new economic frontier, *in* Arribas, R., AM and Mauk, J. eds., Metals, Minerals, and Society: Society of Economic Geologists, p. 157–176.

Kinnaird, J.A., and Nex, P.A., 2015, Platinum-group element (PGE) mineralisation and resources of the Bushveld Complex, *in* Hammond NQ, Hatton C., eds: Council for Geoscience, Pretoria, South Africa, p. 293–341.

Kinnaird, J.A., Hutchinson, D., Schurmann, L., Nex, P.A.M., and de Lange, R., 2005, Petrology and mineralisation of the southern Platreef: northern limb of the Bushveld Complex, South Africa: Mineralium Deposita, v. 40, p. 576–597.

Kitakaze, A., and Sugaki, A., 2004, The phase relations between Fe4.5Ni4.5S8 and Co9S8 in the system Fe-Ni-Co-S at temperatures from 400° to 1100°C: Canadian Mineralogist, v. 42, p. 17–42.

Kitakaze, A., Machida, T., and Komatsu, R., 2016, Phase Relations in the Fe–ni–s System from 875 To 650 °c: The Canadian Mineralogist, v. 54, no. 5, p. 1175–1186.

Li, C., Barnes, S.-J., Makovicky, E., Rose-Hansen, J., and Makovicky, M., 1996, Partitioning of nickel, copper, iridium, rhenium, platinum, and palladium between monosulfide solid solution and sulfide liquid: Effects of composition and temperature: Geochimica et Cosmochimica Acta, v. 60, no. 7, p. 1231–1238.

Liang, Q.-L., Song, X.-Y., Wirth, R., Chen, L.-M., and Dai, Z.-H., 2019, Implications of nano- and micrometer-size platinum-group element minerals in base metal sulfides of the Yangliuping Ni-Cu-PGE sulfide deposit, SW China: Chemical Geology, v. 517, p. 7–21.

Liu, W., Migdisov, A., and Williams-Jones, A., 2012, The stability of aqueous nickel(II) chloride complexes in hydrothermal solutions: Results of UV–Visible spectroscopic experiments: Geochimica et Cosmochimica Acta, v. 94, p. 276–290.

Liu, Y., and Brenan, J., 2015, Partitioning of platinum-group elements (PGE) and chalcogens (Se, Te, As, Sb, Bi) between monosulfide-solid solution (MSS), intermediate solid solution (ISS) and sulfide liquid at controlled fO2–fS2 conditions: Geochimica et Cosmochimica Acta, v. 159, p. 139–161.

Maier, W.D., de Klerk, L., Blaine, J., Manyeruke, T., Barnes, S.-J., Stevens, M.V.A., and Mavrogenes, J.A., 2008, Petrogenesis of contact-style PGE mineralization in the northern lobe of the Bushveld Complex: comparison of data from the farms Rooipoort, Townlands, Drenthe and Nonnenwerth: Mineralium Deposita, v. 43, no. 3, p. 255–280.

Maier, W.D., Abernethy, K.E.L., Grobler, D.F., and Moorhead, G., 2021, Formation of the Flatreef deposit, northern Bushveld, by hydrodynamic and hydromagmatic processes: Mineralium Deposita, v. 56, p. 11–30.

Mansur, E.T., Barnes, S.-J., and Duran, C.J., 2019, Textural and compositional evidence for the formation of pentlandite via peritectic reaction: Implications for the distribution of highly siderophile elements: Geology, v. 47, no. 4, p. 351–354.

Mansur, E.T., Barnes, S.-J., Duran, C.J., and Sluzhenikin, S.F., 2020, Distribution of chalcophile and platinum-group elements among pyrrhotite, pentlandite, chalcopyrite and cubanite from the Noril'sk-Talnakh ores: implications for the formation of platinum-group minerals: Mineralium Deposita, v. 55, no. 6, p. 1215–1232.

Mansur, E.T., Barnes, S.-J., and Duran, C.J., 2021, An overview of chalcophile element contents of pyrrhotite, pentlandite, chalcopyrite, and pyrite from magmatic Ni-Cu-PGE sulfide deposits: Mineralium Deposita, v. 56.

Martin, T., 2018, Characterisation and Spatial Analysis of the Platinum-Grop Mineralogy on Tweefontein Hill & Turfspruit Properties, Northern Bushveld Complex, South Africa: MSc. thesis, Camborne, University of Exeter, 95 p,

McDonald, I., and Holwell, D.A., 2007, Did lower zone magma conduits store PGE-rich sulphides that were later supplied to the Platreef? South African Journal of Geology, v. 110, no. 4, p. 611–616.

McDonald, I., and Holwell, D.A., 2011, Geology of the Northern Bushveld Complex and the Setting and Genesis of the Platreef Ni-Cu-PGE Deposit, in Magmatic Ni-Cu and PGE Deposits: Geology, Geochemistry, and Genesis: Society of Economic Geologists, p. 297–327.

McDonald, I., Holwell, D.A., and Armitage, P.E.B., 2005, Geochemistry and mineralogy of the Platreef and '"Critical Zone"' of the northern lobe of the Bushveld Complex, South Africa: implications for Bushveld stratigraphy and the development of PGE mineralisation: Mineralium Deposita, v. 40, p. 526–549.

McDonald, I., Holwell, D.A., and Wesley, B., 2009, Assessing the potential involvement of an early magma staging chamber in the generation of the Platreef Ni–Cu–PGE deposit in the northern limb of the Bushveld Complex: a pilot study of the Lower Zone Complex at Zwartfontein: Applied Earth Science, v. 118, no. 1, p. 5–20.

van der Merwe, F., Viljoen, F., and Knoper, M., 2012, The mineralogy and mineral associations of platinum group elements and gold in the Platreef at Zwartfontein, Akanani Project, Northern Bushveld Complex, South Africa: Mineralogy and Petrology, v. 106, nos. 1–2, p. 25–38.

van der Merwe, M.J., 2008, The geology and structure of the Rustenburg Layered Suite in the Potgietersrus/Mokopane area of the Bushveld Complex, South Africa: Mineralium Deposita, v. 43, no. 4, p. 405–419.

Mudd, G.M., Jowitt, S.M., and Werner, T.T., 2018, Global platinum group element resources, reserves and mining – A critical assessment: Science of The Total Environment, v. 622–623, p. 614–625.

Mungall, J.E., Andrews, D.R.A., Cabri, L.J., Sylvester, P.J., and Tubrett, M., 2005, Partitioning of Cu, Ni, Au, and platinum-group elements between monosulfide solid solution and sulfide melt under controlled oxygen and sulfur fugacities: Geochimica et Cosmochimica Acta, v. 69, no. 17, p. 4349–4360.

Naldrett, A.J., Asif, M., Scandl, E., Searcy, T., Morrison, G.G., Binney, W.P., and Moore, C., 1999, Platinum-group elements in the Sudbury ores; significance with respect to the

origin of different ore zones and to the exploration for footwall orebodies: Economic Geology, v. 94, no. 2, p. 185–210.

Naldrett, A.J., Asif, M., Krstic, S., and Li, C., 2000, The Composition of Mineralization at the Voisey's Bay Ni-Cu Sulfide Deposit, with Special Reference to Platinum-Group Elements: Economic Geology, v. 95, no. 4, p. 845–865.

Naldrett, A.J., Kinnaird, J., Wilson, A., Yudovskaya, M., McQuade, S., Chunnett, G., and Stanley, C., 2009, Chromite composition and PGE content of Bushveld chromitites: Part 1 – the Lower and Middle Groups: Applied Earth Science, v. 118, nos. 3–4, p. 131–161.

Nex, P.A.M., 2005, The structural setting of mineralisation on Tweefontein Hill, northern limb of the Bushveld Complex, South Africa: Applied Earth Science, v. 114, p. 243–251.

Osbahr, I., Klemd, R., Oberthür, T., Brätz, H., and Schouwstra, R., 2013, Platinum-group element distribution in base-metal sulfides of the Merensky Reef from the eastern and western Bushveld Complex, South Africa: Mineralium Deposita, v. 48, no. 2, p. 211–232.

Palme, H., and O'Neill, H.St.C., 2014, 3.1 - Cosmochemical Estimates of Mantle Composition, in Holland, H.D. and Turekian, K.K. eds., Treatise on Geochemistry (Second Edition): Oxford, Elsevier, p. 1–39.

Piercey, S., 2014, Modern Analytical Facilities 2: A Review of Quality Assurance and Quality Control (QA/QC) Procedures for Lithogeochemical Data: Geoscience Canada: Journal of the Geological Association of Canada / Geoscience Canada: journal de l'Association Géologique du Canada, v. 41, no. 1, p. 75–88.

Piña, R., Gervilla, F., Helmy, H., Fonseca, R.O.C., and Ballhaus, C., 2020, Partition behavior of platinum-group elements during the segregation of arsenide melts from sulfide magma: American Mineralogist, v. 105, no. 12, p. 1889–1897.

Queffurus, M., and Barnes, S.-J., 2015, A review of sulfur to selenium ratios in magmatic nickel–copper and platinum-group element deposits: Ore Geology Reviews, v. 69, p. 301–324.

Scoon, R.N., and Teigler, B., 1994, Platinum-group element mineralization in the critical zone of the western Bushveld Complex; I, Sulfide poor-chromitites below the UG-2: Economic Geology, v. 89, no. 5, p. 1094–1121.

Sharman-Harris, E.R., Kinnaird, J.A., Harris, C., and Horstmann, U.E., 2005, A new look at sulphide mineralisation of the northern limb, Bushveld Complex: a stable isotope study: Applied Earth Science, v. 114, no. 4, p. 252–263.

Smith, J.W., Holwell, D.A., and McDonald, I., 2014, Precious and base metal geochemistry and mineralogy of the Grasvally Norite–Pyroxenite–Anorthosite (GNPA) member, northern Bushveld Complex, South Africa: implications for a multistage emplacement: Mineralium Deposita, v. 49, no. 6, p. 667–692.

Smith, J.W., Holwell, D.A., McDonald, I., and Boyce, A.J., 2016, The application of S isotopes and S/Se ratios in determining ore-forming processes of magmatic Ni–Cu–PGE sulfide deposits: A cautionary case study from the northern Bushveld Complex: Ore Geology Reviews, v. 73, p. 148–174.

Sullivan, N.A., Zajacz, Z., Brenan, J.M., and Tsay, A., 2022, The solubility of platinum in magmatic brines: Insights into the mobility of PGE in ore-forming environments: Geochimica et Cosmochimica Acta, v. 316, p. 253–272.

Thériault, R.D., Barnes, S.-J., and Severson, M.J., 1997, The influence of country-rock assimilation and silicate to sulfide ratios (R factor) on the genesis of the Dunka Road Cu – Ni – platinum-group element deposit, Duluth Complex, Minnesota: Canadian Journal of Earth Sciences, v. 34, no. 4, p. 375–389.

Tolstykh, N., Brovchenko, V., Rad'ko, V., Shapovalova, M., Abramova, V., and Garcia, J., 2022, Rh, Ir, and Ru Partitioning in the Cu-Poor IPGE Massive Ores, Talnakh Intrusion, Skalisty Mine, Russia: Minerals, v. 12, no. 1, p. 18.

Van der Merwe, M.J., 1976, The layered sequence of the Potgietersrus Limb of the Bushveld Complex: Economic Geology, v. 71, no. 7, p. 1337–1351.

Yudovskaya, M., Kinnaird, J., Naldrett, A.J., Mokhov, A.V., McDonald, I., and Reinke, C., 2011, FACIES VARIATION IN PGE MINERALIZATION IN THE CENTRAL PLATREEF OF THE BUSHVELD COMPLEX, SOUTH AFRICA: The Canadian Mineralogist, v. 49, no. 6, p. 1349–1384.

Yudovskaya, M.A., Kinnaird, J.A., Grobler, D.F., Costin, G., Abramova, V.D., Dunnett, T., and Barnes, S.-J., 2017, Zonation of Merensky-Style Platinum-Group Element Mineralization in Turfspruit Thick Reef Facies (Northern Limb of the Bushveld Complex): Economic Geology, v. 112, no. 6, p. 1333–1365.

Zeh, A., Ovtcharova, M., Wilson, A.H., and Schaltegger, U., 2015, The Bushveld Complex was emplaced and cooled in less than one million years – results of zirconology, and geotectonic implications: Earth and Planetary Science Letters, v. 418, p. 103–114.

Figures

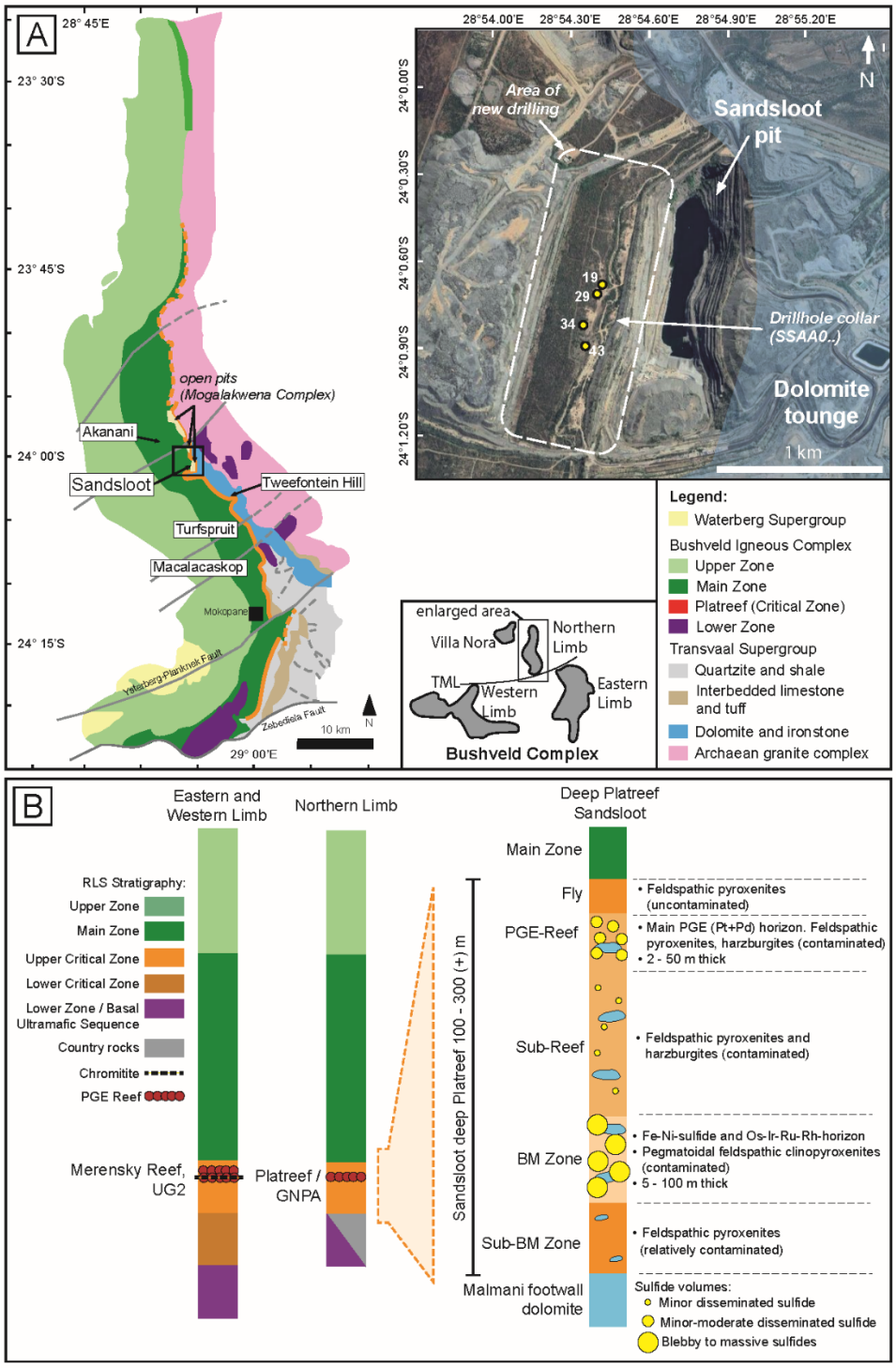

Figure 1. *(A) Geological map of the Northern Limb with Sandsloot and other localities referenced annotated (adapted from van der Merwe, 1976 and further modified using adaptions from Ashwal et al., 2005; Van der Merwe et al., 2012; Kinnaird and McDonald, 2018). Satellite image of the area of drilling intersecting the down-dip Platreef is also shown. (B) Simplified stratigraphic log of the Rustenburg Layered Suite (RLS) in the Eastern and Western Limb correlated to the Northern Limb (after White, 1994) and the deep Platreef at Sandsloot (after Thompson et al., in review).*

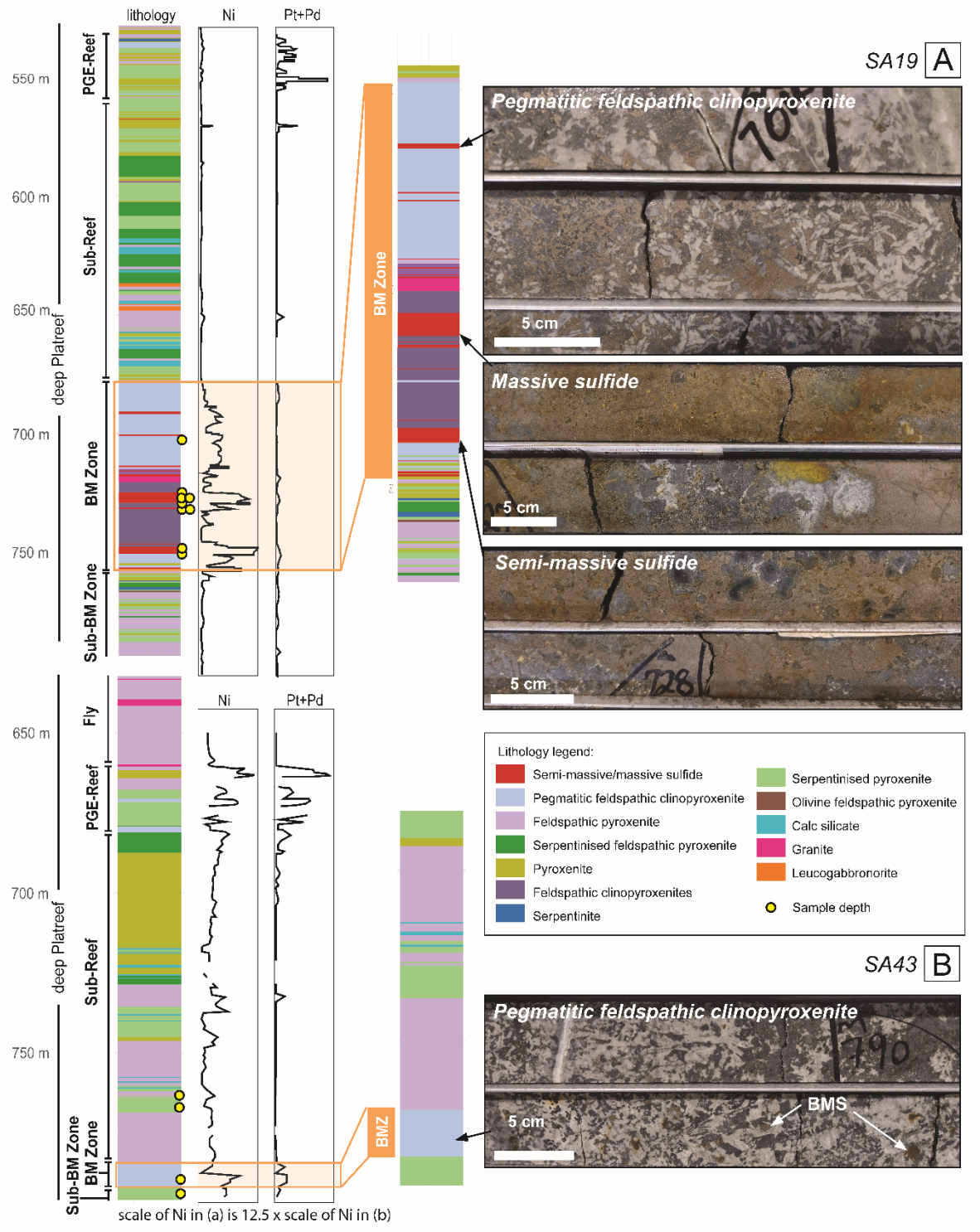

Figure 2. *Downhole stratigraphic and lithological logs alongside downhole metal geochemistry (Ni and Pt+Pd) of (A) SA19 and (B) SA43 through the deep Platreef at Sandsloot, the BM Zone is highlighted. Scale for Ni and Cu are not the same in (A) and (B). Photographs of core in the BM Zone is also shown. Data for stratigraphic and assay logs was provided by Anglo American.*

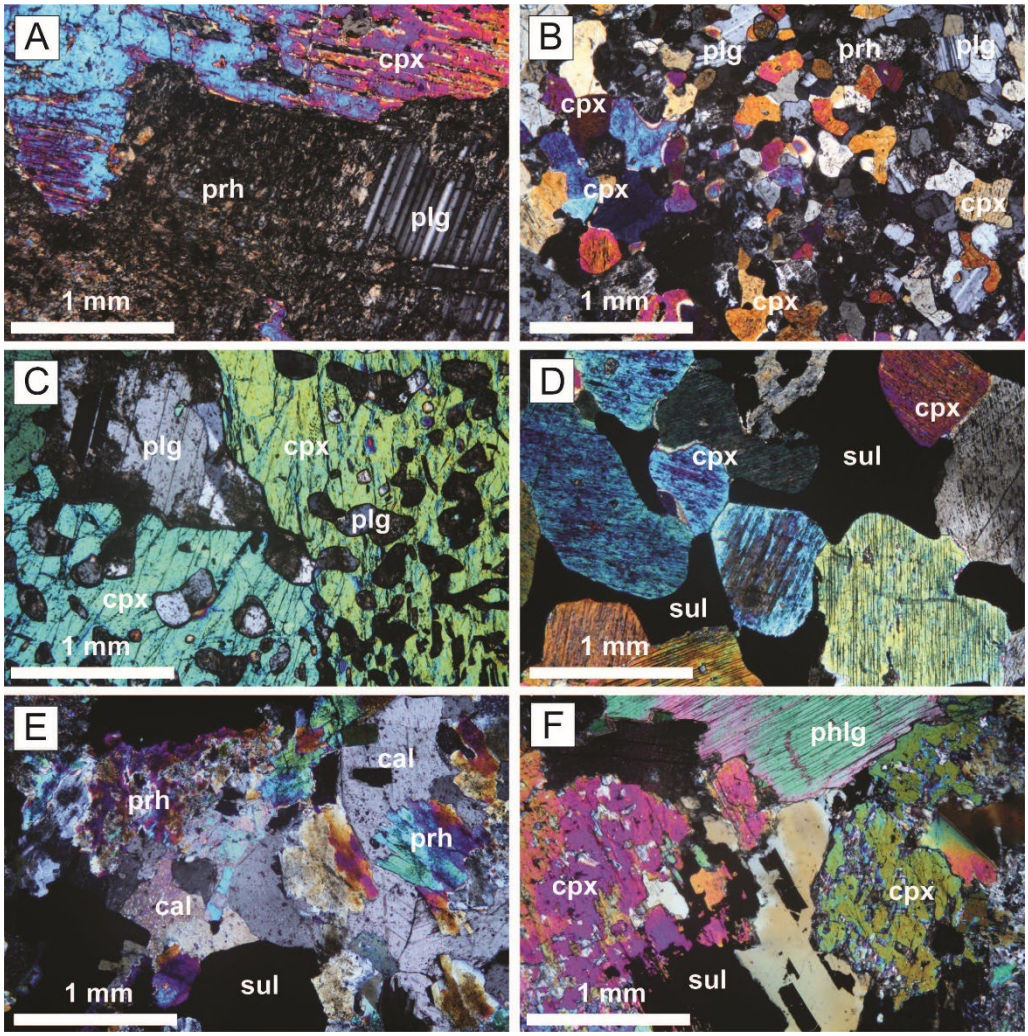

Figure 3. *Photomicrographs of typical textures in the BM Zone in cross polarised transmitted light. (A) pegmatoidal clinopyroxene and plagioclase, plagioclase is near totally replaced by prehnite; (B) fine grained amoeboid granoblastic plagioclase and clinopyroxene; (C) coarse grained clinopyroxene with plagioclase intergrowths; (D) medium grained rounded clinopyroxene, with sulfide; (E) calcite and prehnite alteration; (F) phlogopite, sulfide and hornblende within clinopyroxenite. Abbreviations: Cpx = clinopyroxene, preh = prehnite, plg = plagioclase, sul = sulfide, cal = calcite, phlg = phlogopite.*

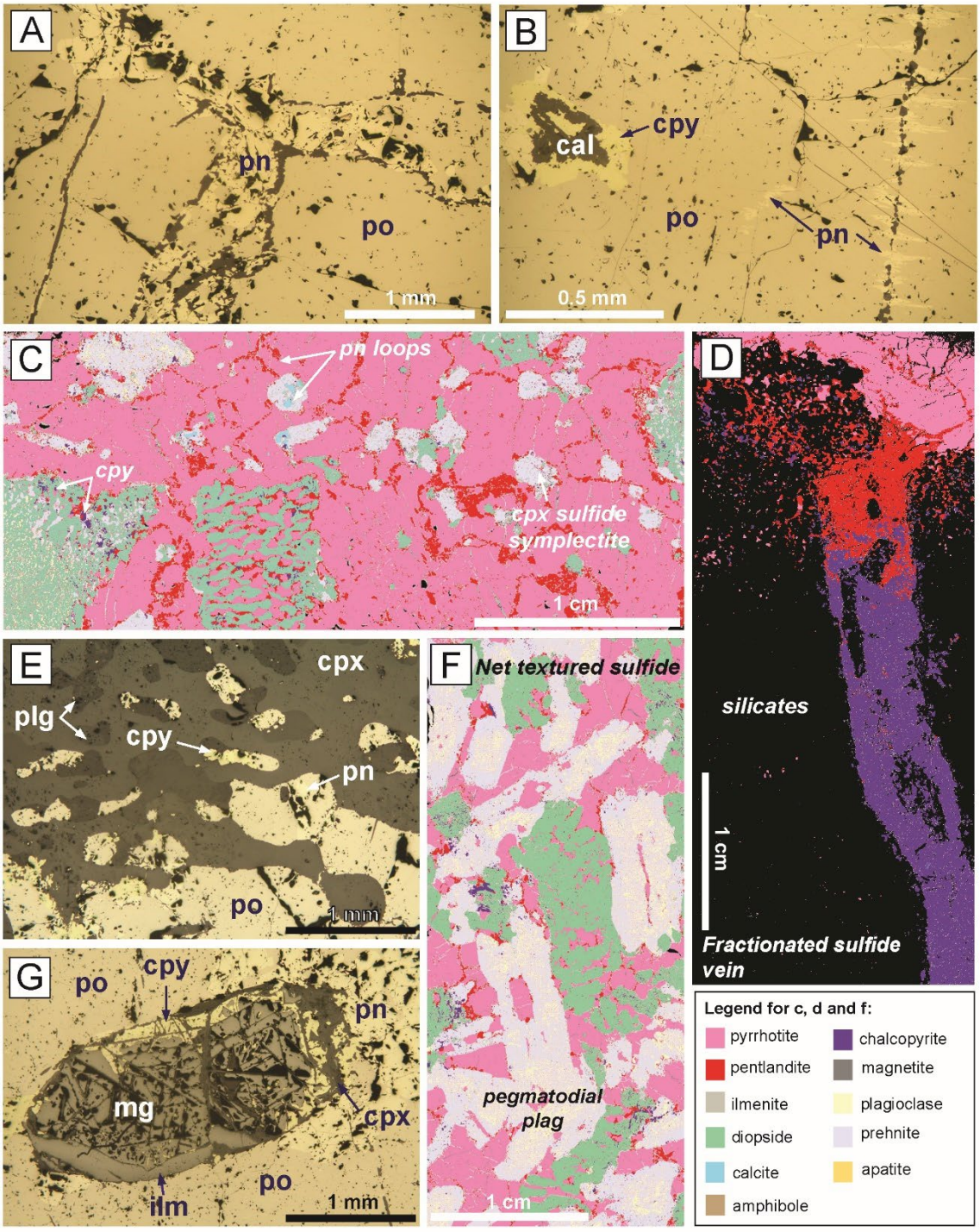

Figure 4. *(A-B, E, G) Photomicrographs and (C-D, F) mineral maps of typical textures in the semi-massive to massive sulfides in the BM Zone. (A) Pentlandite loops within pyrrhotite, (B) pentlandite exsolution within pyrrhotite and chalcopyrite around calcite, (C) symplectite sulfide-silicate texture with pentlandite loops and chalcopyrite separated and towards the boundary of the symplectite, (D) fractionated sulfide vein, (E) symplectite sulfide and silicates, including clinopyroxene and plagioclase variably altered to prehnite, (F) semi-massive net textured sulfide with coarse grained plagioclase laths, and (G) coarse grained magnetite and ilmenite with chalcopyrite around its boundary, hosted within massive sulfide. Abbreviations: po = pyrrhotite, pn = pentlandite, cpy = chalcopyrite, cal = calcite, cpx = clinopyroxene, plg = plagioclase, mg = magnetite, ilm = ilmenite.*

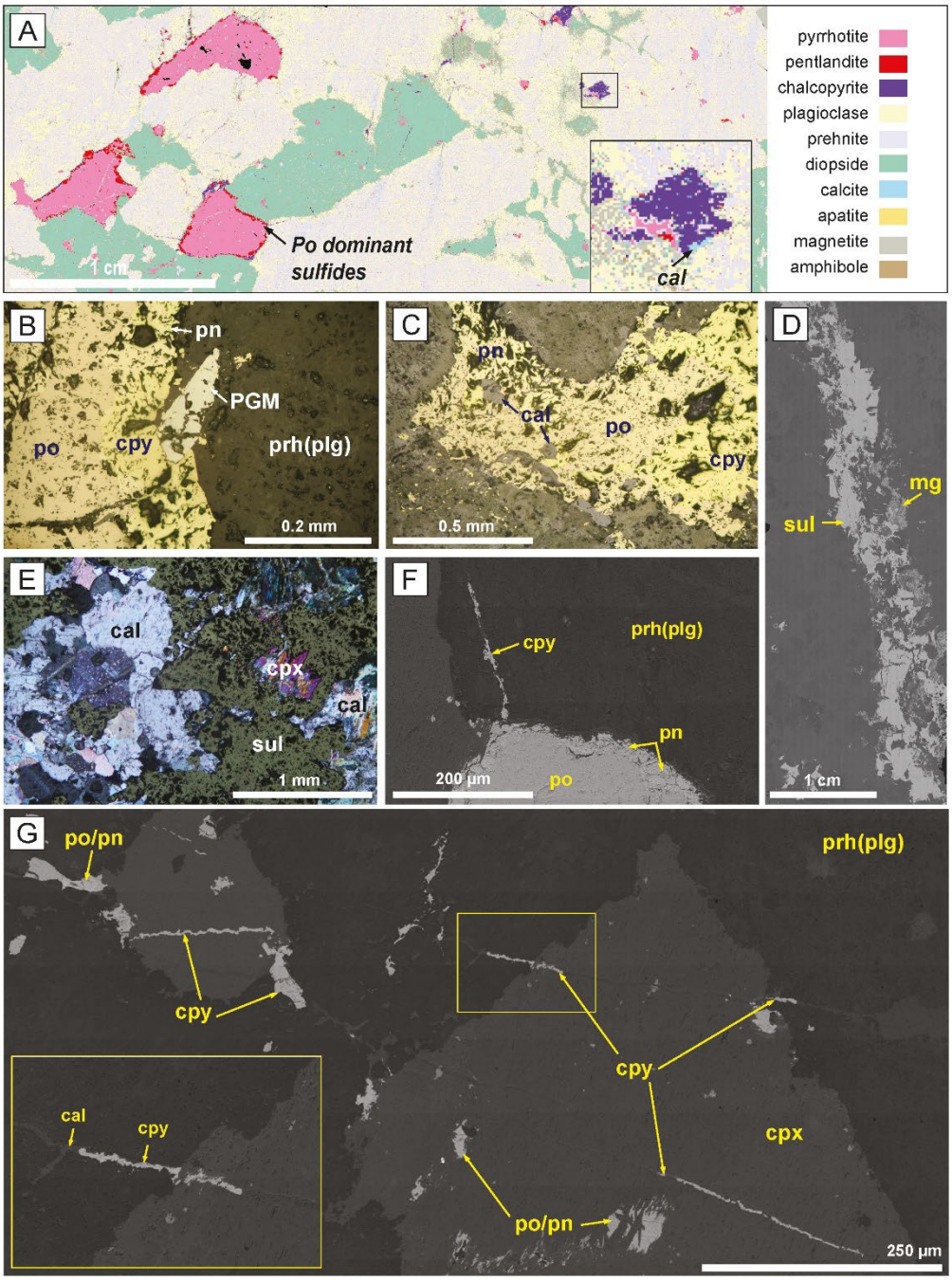

Figure 5. *Photomicrographs, BSE images and mineral maps of (A-C) disseminated/blebby and (D-G) vein sulfide textures in the BM Zone. (A) Mineral map of blebby sulfides, highlighting the pyrrhotite-rich nature of the sulfide ores. Also note the association of calcite with chalcopyrite-rich sulfide blebs. Photomicrograph of (B) pentlandite and chalcopyrite rims around pyrrhotite and (C) pyrrhotite, chalcopyrite, pentlandite sulfide bleb containing calcite inclusions. (D) BSE image of sulfide (pyrrhotite, pentlandite and chalcopyrite) vein with magnetite, (E) photomicrograph showing enlarged view of sulfide vein in (D), showing calcite hosted alongside sulfide in the vein, vein is wider than the view diameter, (F) BSE image of separation of chalcopyrite from pentlandite and pyrrhotite, (G) BSE image of chalcopyrite ± calcite veins crosscutting silicates, pyrrhotite and pentlandite occurs as blebs which are overprinted by secondary silicates. Abbreviations: po = pyrrhotite, cpy = chalcopyrite, pn = pentlandite, cal = calcite, prh(plg) = prehnite altered plagioclase, sul = sulfide, mg = magnetite, cpx = clinopyroxene.*

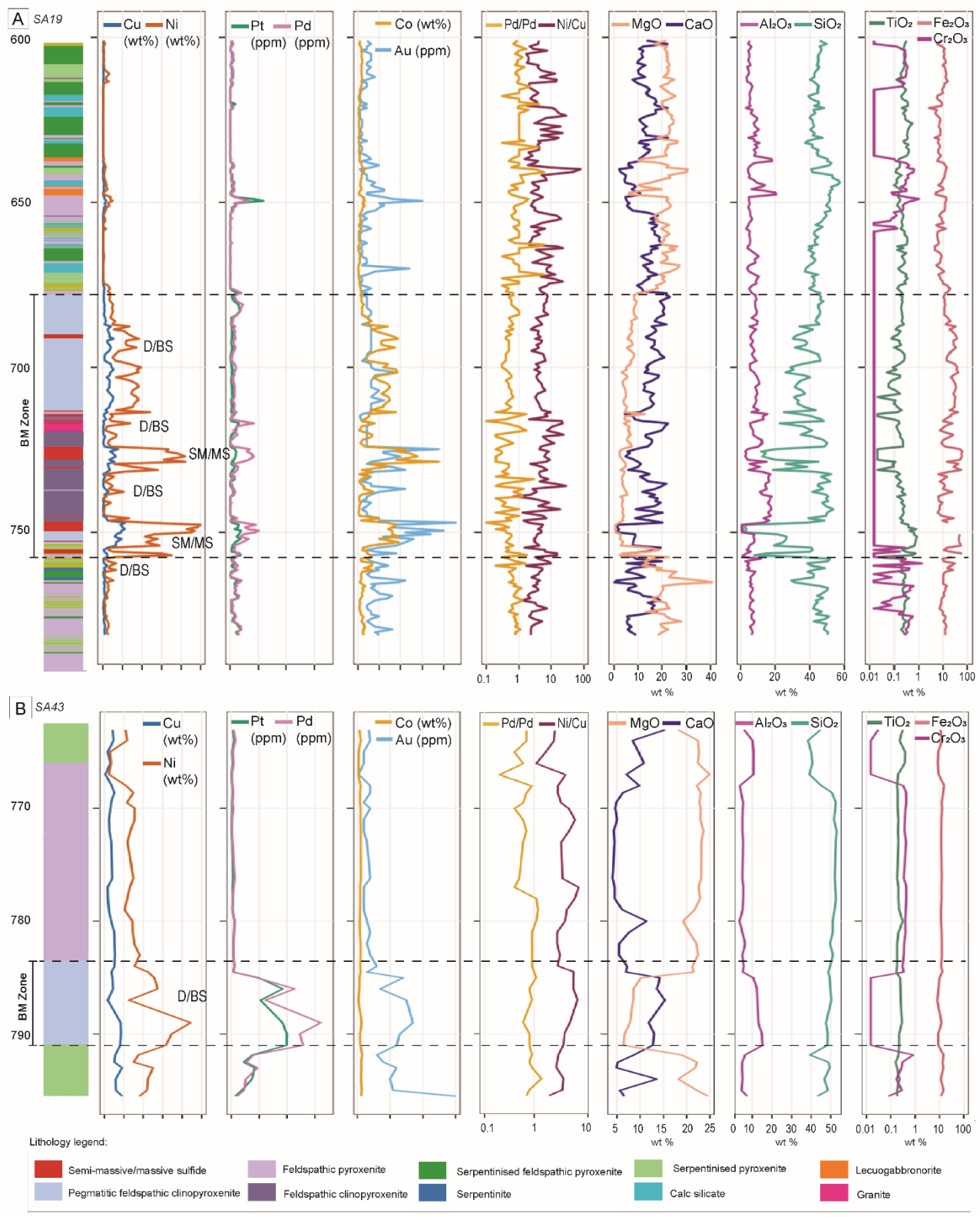

Figure 6. *Downhole stratigraphic, lithological, geochemical and relative metal contents plots of (A) SA19 and (B) SA43 through the BM Zone, with the overlying Sub-Reef and underlying Sub-BM Zone also shown. The BM Zone in (A) intersects massive/semi-massive sulfides as well as disseminated/blebby sulfides, while the BM Zone in (B) only intersects blebby/disseminated sulfides. Geochemistry was provided by Anglo American. Abbreviations: D/BS = disseminated/blebby sulfides, SM/MS = semi-massive/massive sulfides.*

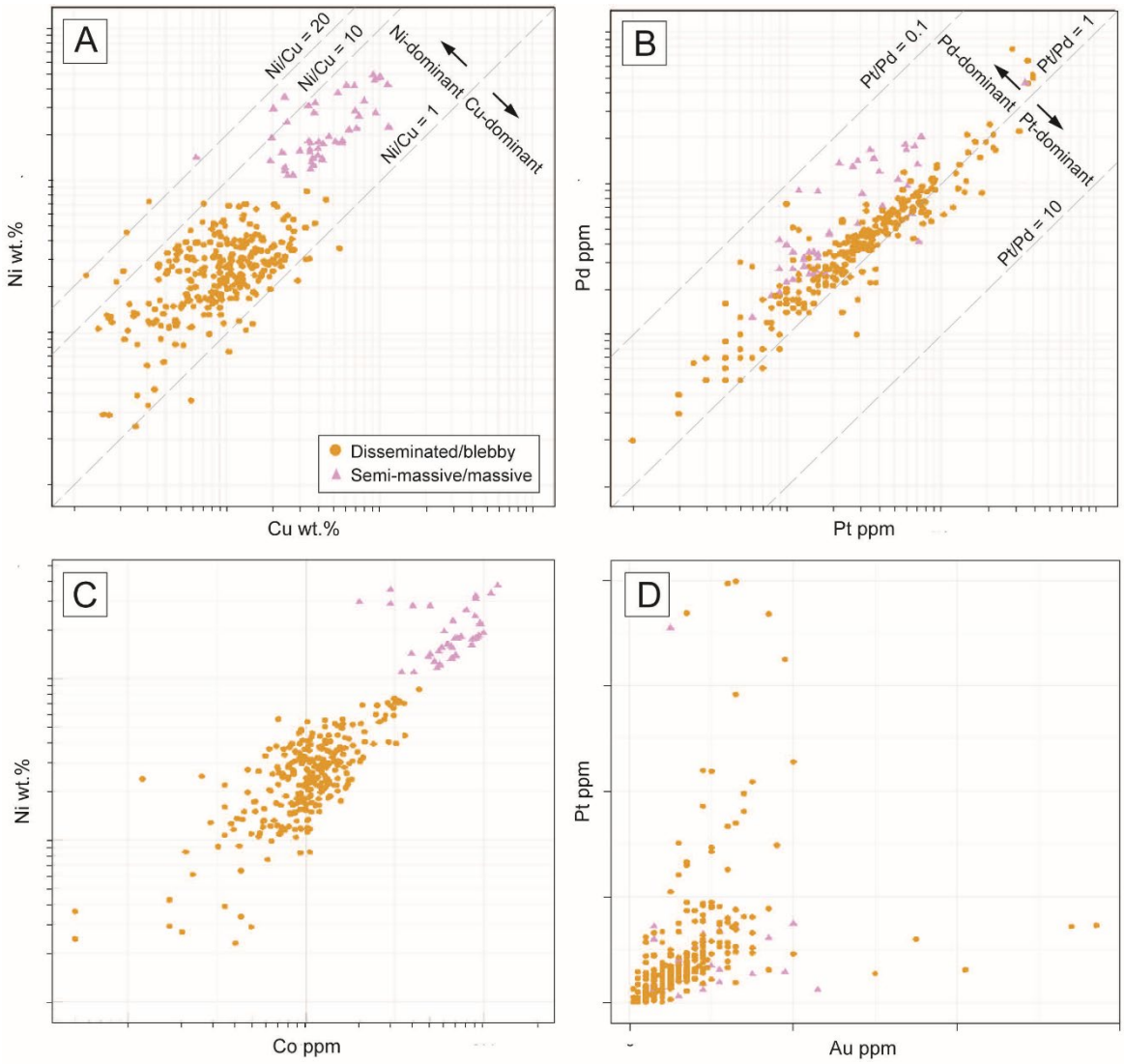

Figure 7. *X-Y plots of whole-rock chalcophile metals in the BM Zone in the deep Platreef at Sandsloot. (A) Cu vs Ni (logged scale), (B) Pt vs Pd (logged scale), (C) Co vs Ni (logged scale), (D) Au vs Pt. Geochemistry was provided by Anglo American.*

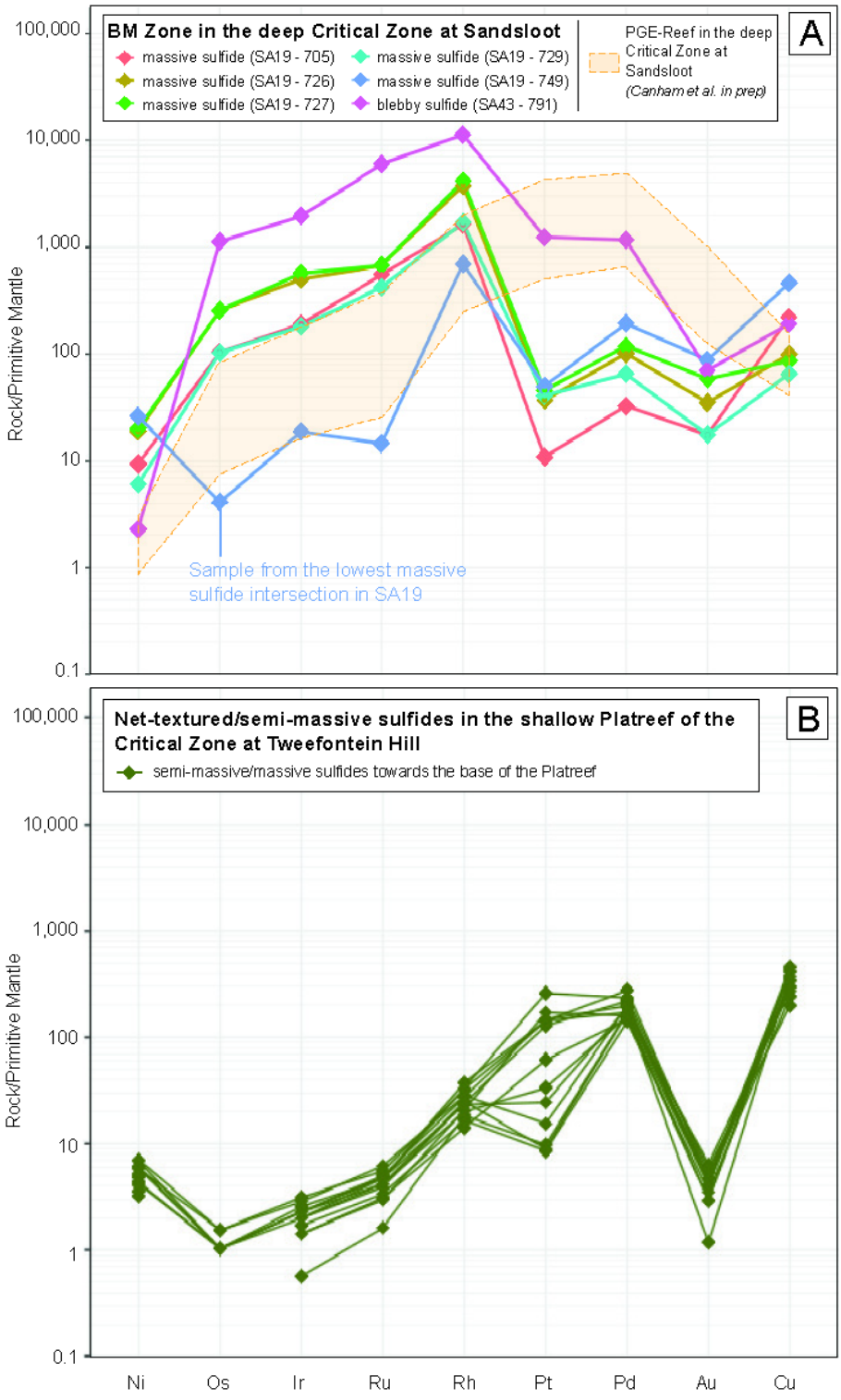

Figure 8. *Whole-rock PGE+Cu+Ni normalised to primitive mantle for (A) the BM Zone in the deep Platreef at Sandsloot and (B) net-textured and semi-massive sulfides towards the base of the shallow Platreef at Tweefontein Hill. The field for the overlying PGE-Reef in the deep Platreef at Sandsloot (from Canham et al. in prep) is also shown on (A). Primitive mantle values are from Palme and O'Neill (2014).*

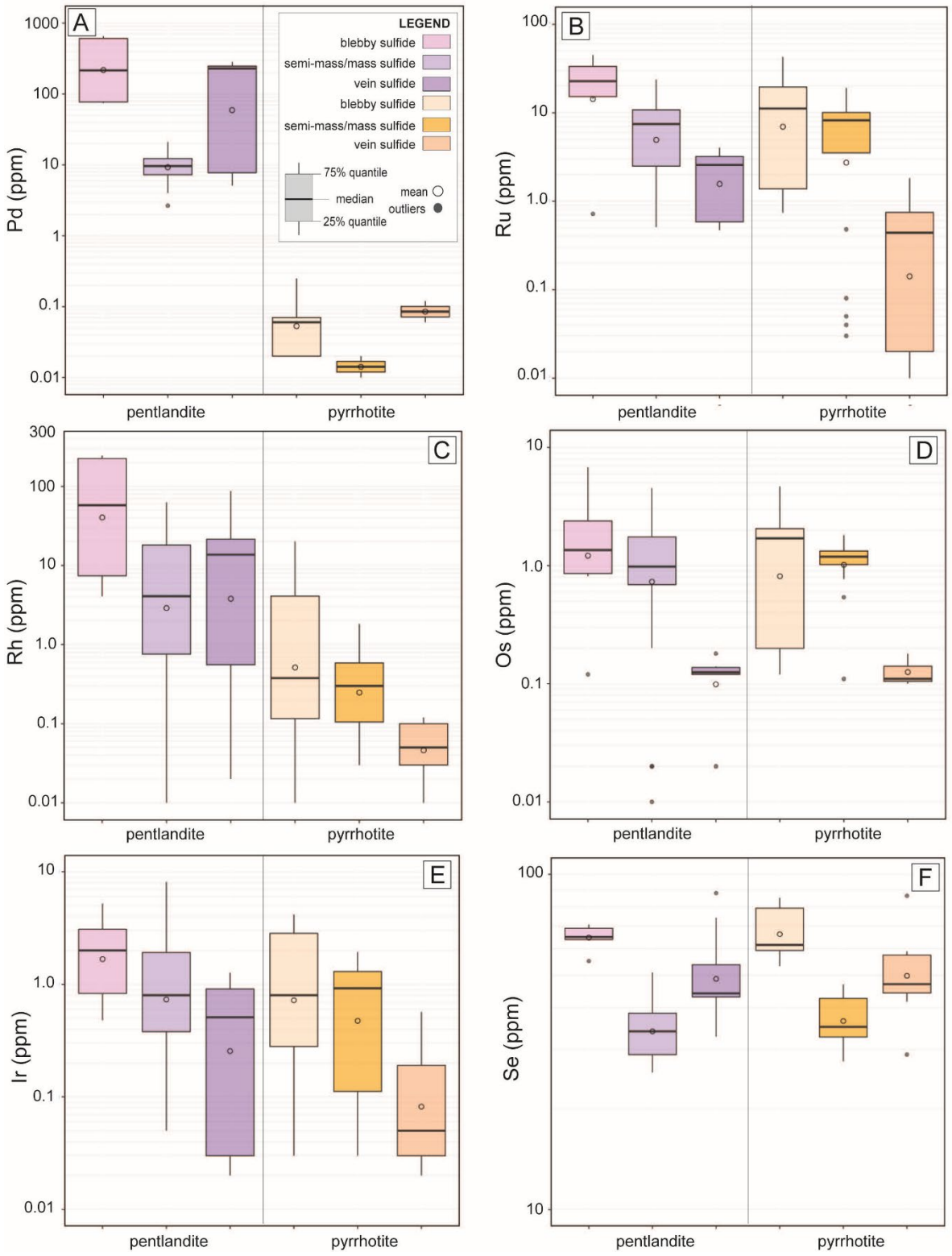

Figure 9. *Box and whisker plots of (A) Pd, (B) Ru, (C) Rh, (D) Os, (E) Ir and (F) Se contents in pentlandite and pyrrhotite in the BM Zone in the deep Platreef at Sandsloot. Each box represents a different sulfide texture.*

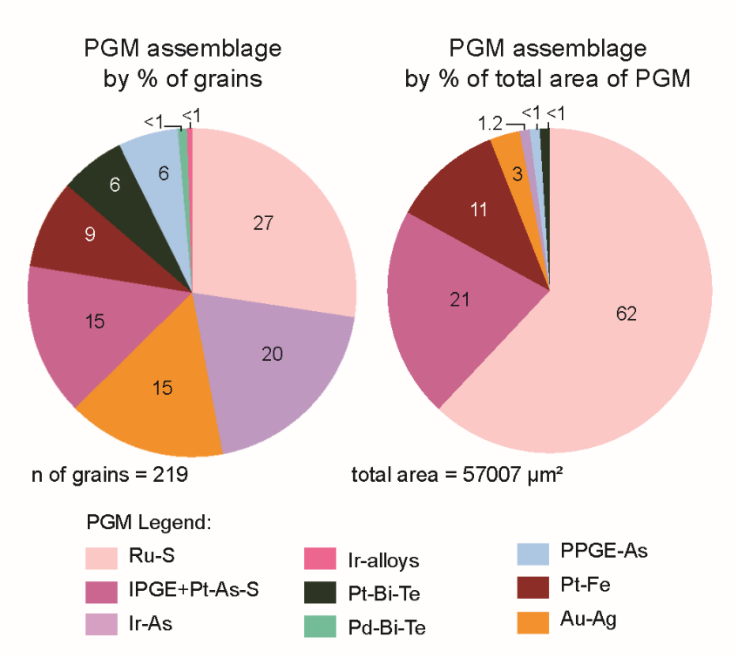

Figure 10. *Pie charts of the PGM assemblage of the BM Zone in the deep Platreef at Sandsloot.*

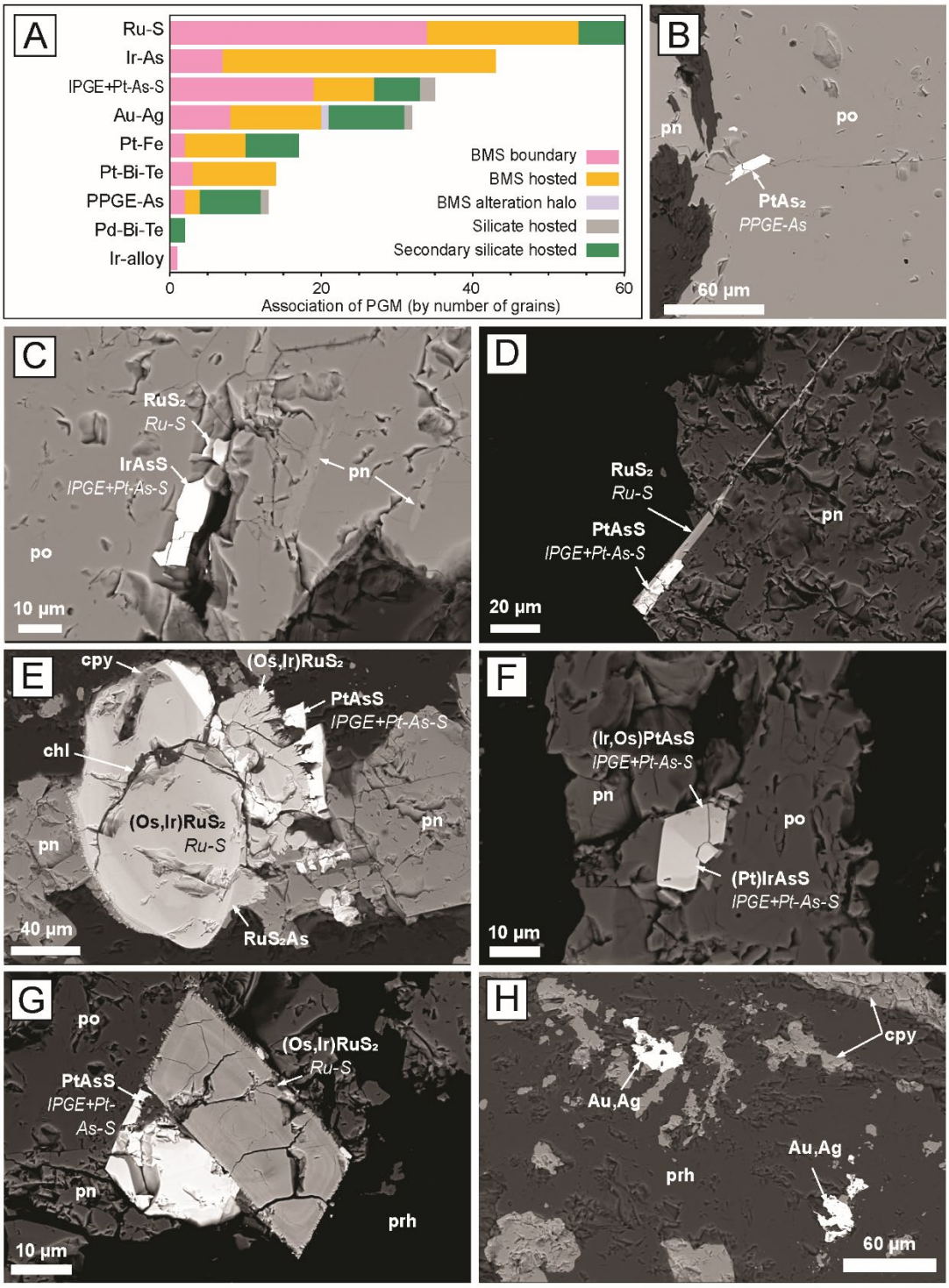

Figure 11. *(A) Stacked bar chart of the association of each PGM type in the BM Zone in the deep Platreef at Sandsloot and (B-H) photomicrographs of typical PGM textures. The formula of the PGM is given in bold and its associated PGM group is given underneath in italics. (B) $PtAs_2$ hosted in pyrrhotite, (C) IrAsS and RuS_2 hosted within pyrrhotite containing pentlandite flames, (D) bladed PtAsS and RuS_2, (E) coarse grained zoned Os, Ir-bearing RuS_2 and PtAsS hosted on boundary of pentlandite, chlorite (chl) crosscuts the PGM, (F) PtAsS and Pt-bearing IrAsS within sulfide, (G) PtAsS and euhedral oscillatory zoned Os, Ir-bearing RuS_2 on sulfide prehnite boundary, (H) electrum (Au,Ag) associated with chalcopyrite within prehnite altered plagioclase. Abbreviations: po = pyrrhotite, pn = pentlandite, cpy = chalcopyrite, prh = prehnite.*

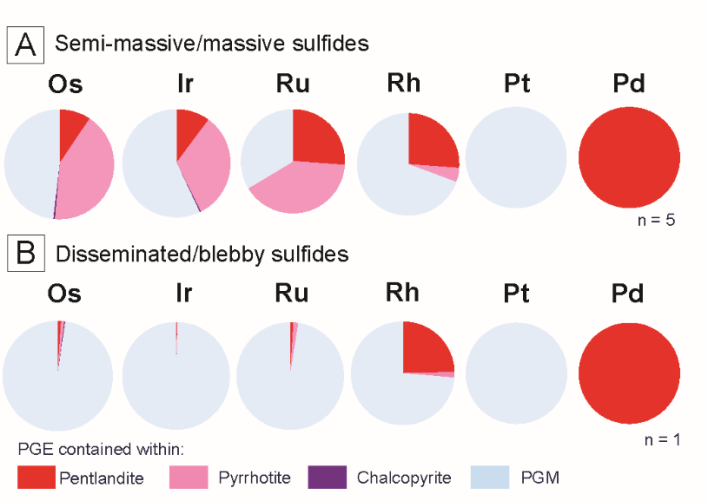

Figure 12. *Pie charts summarising mass balance of PGE held contained within sulfide and PGM within (A) semi-massive/massive sulfides and (B) disseminated/blebby sulfides in the BM Zone in the deep Platreef at Sandsloot. n = number of samples.*

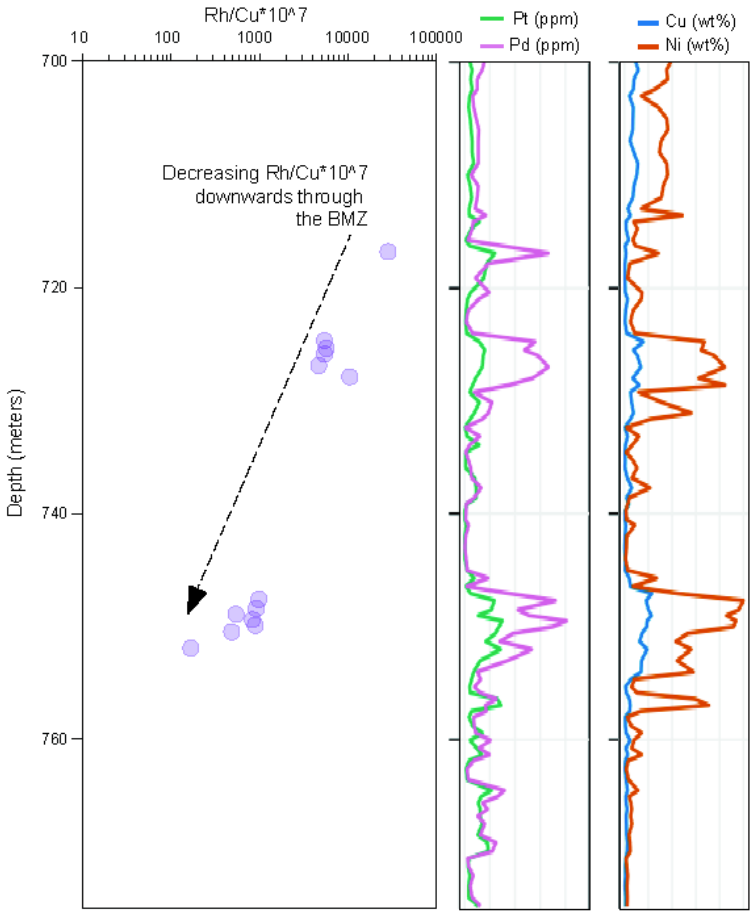

Figure 13. *Vertical profiles downhole of SA19 through the BM Zone, showing the variation of Rh/Cu*10^7 with depth. The variation of Ni, Cu, Pt and Pd downhole is also shown for reference.*

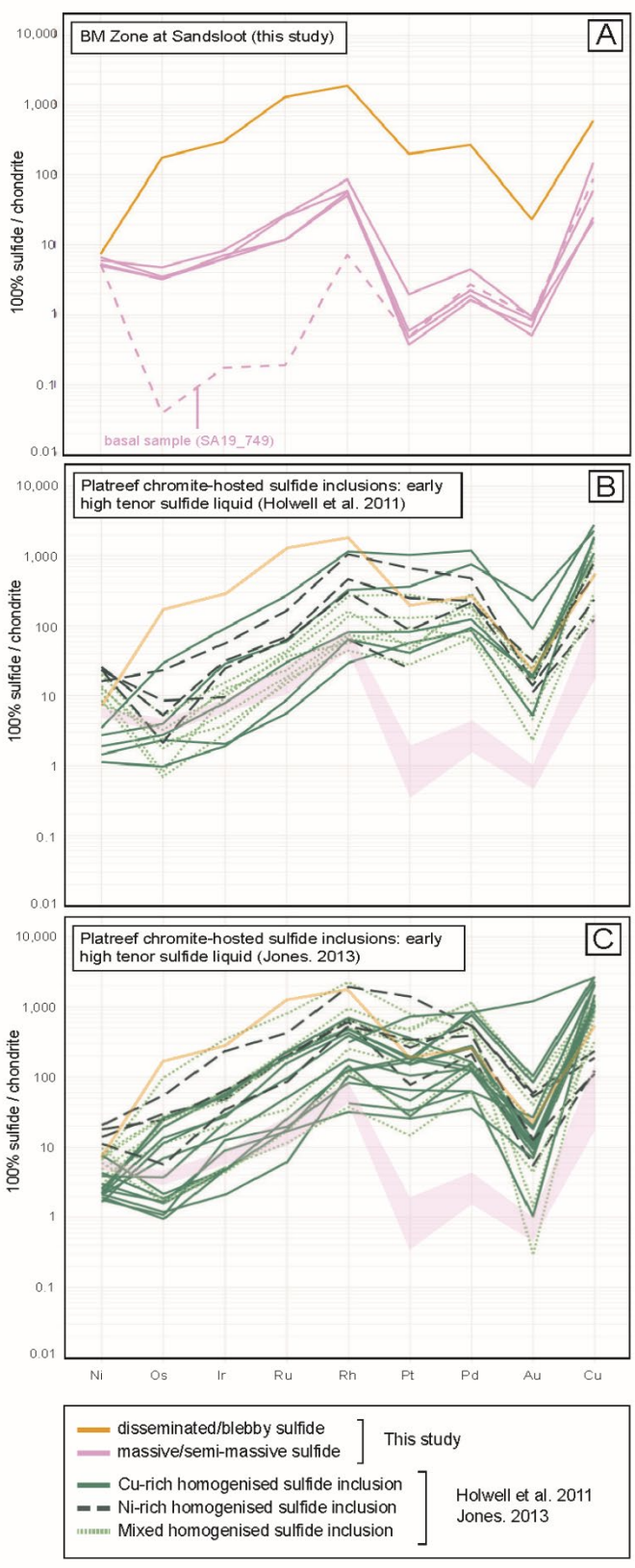

Figure. 14. *Chondrite normalised Cu, Ni and PGE tenor (Ni, Cu and PGE in 100% sulfide) diagrams for the (A) BM Zone (this study) compared to (B and C) homogenised chromite-hosted sulfide inclusions from the shallow Platreef (taken from Holwell et al. 2011; Jones 2013). The chromite-hosted sulfide inclusions have been divided into Cu-rich, Ni-rich and mixed inclusions. Chondrite values are from Fischer-Gödde et al. (2010).*

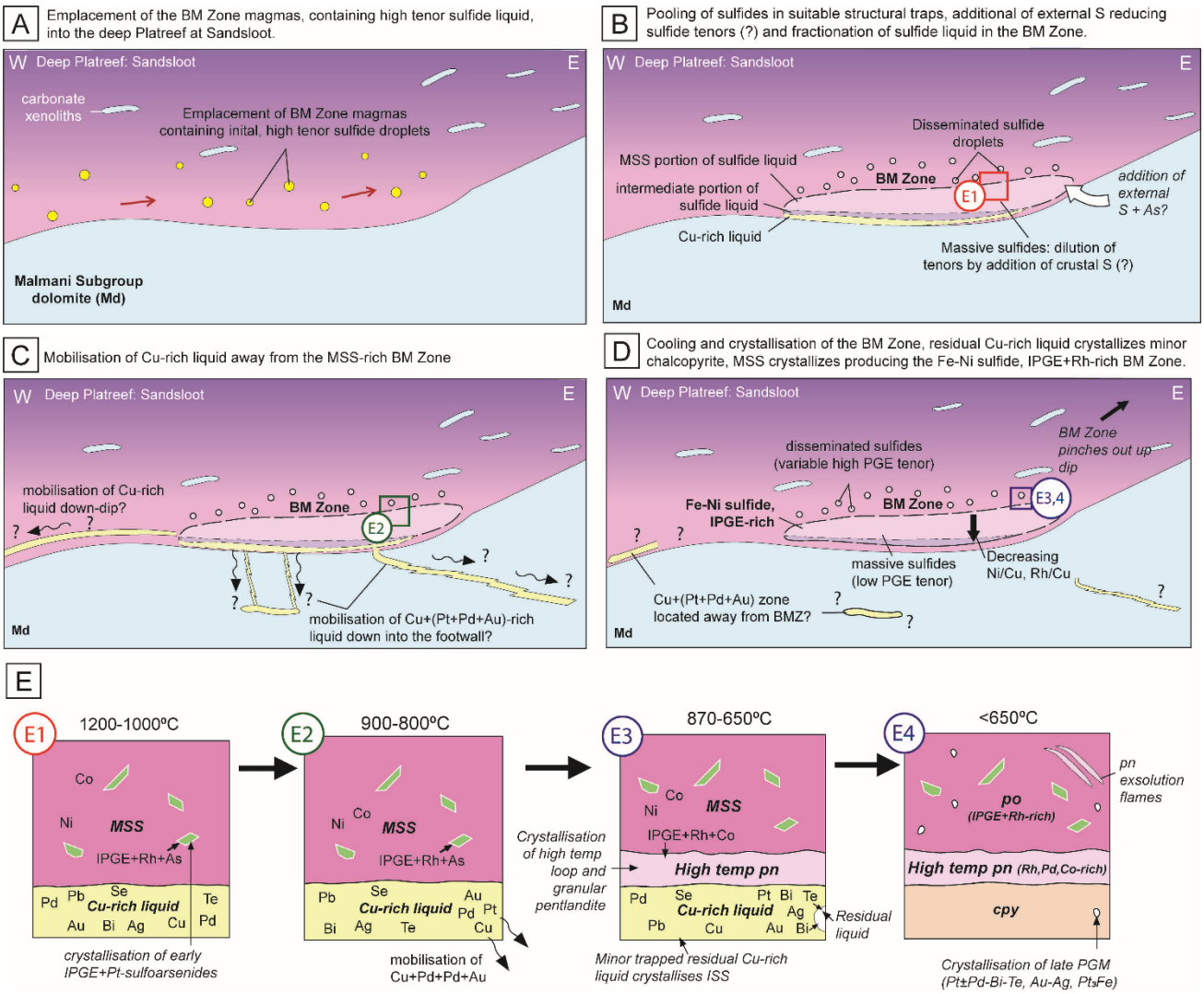

Figure 15. *Schematic illustration depicting the processes of sulfide fractionation in the formation of PGM and sulfides within the BM Zone in the deep Platreef at Sandsloot. (A-D) Illustrate the emplacement of a high tenor sulfide liquid into the deep Platreef. This subsequently fractionates and produces the BM Zone, which is representative of the MSS-portion of the sulfide liquid. The sulfide liquid fractionated downwards through the BM Zone and the residual Cu(+Pt-Pd-Au)-rich liquid was likely mobilised downwards and away. (E) Shows the crystallization history of the sulfide liquid, including (E1) formation of high temperature IPGE+Pt-sulfoarsenides, (E2) separation of the Cu-rich liquid from MSS, (E3) formation of high-temperature pentlandite via peritectic reaction and finally, (E4) low temperature exsolution of pyrrhotite and minor pentlandite from MSS, and minor chalcopyrite from ISS.*

Table 1. *Table summarising the lithology and sulfide texture of samples from this study. Sulfide Texture 1 refers to the sulfide texture group the sample is assigned, Sulfide Texture 2 is a more detailed description of the sulfide texture. BMZ = BM Zone. w*

Hole	Depth (m)	Zone	Lithology	Sulfide Texture 1	Sulfide Texture 2	Pt+Pd+Au grade	IPGE+Rh grade
SA19	705	BMZ	BMS pegmatoidal feldspathic clinopyroxenite	semi-massive/massive	net textured	Low	High
SA19	724	BMZ	BMS feldspathic clinopyroxenite	semi-massive/massive	semi-massive	Low	NA
SA19	726A	BMZ	BMS feldspathic clinopyroxenite	semi-massive/massive	massive symplectic	Low	High
SA19	726B	BMZ	BMS pegmatoidal feldspathic clinopyroxenite	semi-massive/massive	semi-massive symplectite	Low	High
SA19	727	BMZ	BMS feldspathic pyroxenite	semi-massive/massive	vein (fractionated)	Low	High
SA19	729A	BMZ	BMS feldspathic clinopyroxenite	semi-massive/massive	semi-massive symplectite	Low	High
SA19	729B	BMZ	BMS sulfide feldspathic pyroxenite	semi-massive/massive	net textured	Low	High
SA19	749	BMZ	Massive BMS	semi-massive/massive	massive	Low	Low
SA19	750	BMZ	BMS feldspathic clinopyroxenite	semi-massive/massive	semi-massive symplectite	Low	NA
SA29	761	BMZ	Clinopyroxenite	disseminated/blebby	disseminated/blebby	Moderate	NA
SA34	769	BMZ	Serpentinised feldspathic clinopyroxenite	disseminated/blebby	disseminated	Low	NA
SA34	772	BMZ	Feldspathic clinopyroxenite	disseminated/blebby	blebby	Low	NA
SA34	780	BMZ	Pegmatoidal feldspathic clinopyroxenite	disseminated/blebby	disseminated	Low	NA
SA43	764	above BMZ	Pyroxenite (altered)	disseminated/blebby	blebby	Low	NA
SA43	769	Above BMZ	Pyroxenite	disseminated/blebby	disseminated	Low	NA
SA43	791	BMZ	Pegmatoidal feldspathic clinopyroxenite	disseminated/blebby	blebby, minor vein	High	Very high
SA43	794	Sub-BMZ	Pyroxenite (altered)	vein	vein (with calcite)	Moderate	NA

Table 2. *Ratios of trace elements and PGE for the BM Zone at Sandsloot (full trace element data is available in Appendix Table. A3). NA = data not available, as full 6PGE was not analysed. BMZ = BM Zone, mod = moderate, min = minimum, maj = major, Alt = alteration,*

Hole	*Depth (m)*	*Zone*	*Alt*	*Sulfide texture*	IPGE/ PPGE	IPGE +Rh/ Pt+Pd	Pt/ Pd	Ni/Cu	Au/Pd	Pd/ Ir	Rh/ Ir	Rh/Pd	(Rh/Cu) *10^7	S/Se	S (%)
SA19	**705**	**BMZ**	**maj**	**semi-massive/massive**	2.26	22.42	0.35	3.94	0.13	0.35	2.93	8.36	4416	5702	9.58
SA19	**724**	**BMZ**	**maj**	**semi-massive/massive**	NA	NA	0.21	10.50	0.14	NA	NA	3.08	15448	8830	22.87
SA19	**726A/B**	**BMZ**	**min**	**semi-massive/massive**	1.41	12.21	0.39	17.79	0.08	0.41	2.56	6.25	22663	8393	25.77
SA19	**727**	**BMZ**	**mod**	**semi-massive/massive (vein)**	1.29	10.84	0.41	21.62	0.12	0.43	2.50	5.88	28902	7691	25.61
SA19	**729A/B**	**BMZ**	**mod**	**semi-massive/massive**	1.48	8.01	0.67	8.66	0.06	0.73	3.20	4.41	15573	7394	6.95
SA19	**749**	**BMZ**	**mod**	**semi-massive/massive**	0.07	0.59	0.28	5.34	0.11	20.83	12.74	0.61	910	8175	34.17
SA19	**750**	**BMZ**	**min**	**semi-massive/massive**	NA	NA	0.64	5.59	0.18	NA	NA	0.38	627	6567	13.07
SA29	**761**	**BMZ**	**min**	**disseminated/blebby**	NA	NA	1.28	2.13	0.06	0.81	0.62	0.76	6736	5184	2.54
SA34	**769**	**BMZ**	**maj**	**disseminated/blebby**	NA	NA	0.81	2.36	0.04	NA	NA	0.06	684	4500	0.72
SA34	**772**	**BMZ**	**mod**	**disseminated/blebby**	NA	NA	0.79	1.70	0.04	NA	NA	NA	NA	4444	0.80
SA34	**780**	**BMZ**	**mod**	**disseminated/blebby**	NA	NA	0.82	1.82	0.11	NA	NA	NA	NA	2636	0.29
SA43	**764**	**above BMZ**	**maj**	**disseminated/blebby**	NA	NA	0.69	2.68	0.14	NA	NA	NA	NA	5604	2.69
SA43	**769**	**above BMZ**	**min**	**disseminated/blebby**	NA	NA	0.67	2.54	0.33	NA	NA	NA	NA	2000	0.06
SA43	**791**	**BMZ**	**mod**	**disseminated/blebby**	1.78	3.89	1.14	1.10	0.01	1.22	1.98	1.63	35065		2.01
SA43	**794**	**Sub-BMZ**	**maj**	**vein**	NA	NA	1.43	2.98	0.10	NA	NA	0.90	12047	6361	2.29

Table 3. *Cu, Ni and PGE+Au in 100% sulfide in the BM Zone at Sandsloot. Calculated following the formula of Barnes and Lightfoot (2005).*

HOLE ID	SAMPLE ID	ZONE	Sulfide Texture	Ni wt.%	Cu wt.%	Pd ppm	Pt ppm	Rh ppm	Ir ppm	Os ppm	Ru ppm	Au ppm
SSAA019	SA019_705	BMZ	Semi-massive/massive	6.97	1.77	0.93	0.33	7.80	2.66	1.61	16.24	0.12
SSAA019	SA019_724	BMZ	Semi-massive/massive	4.94	0.47	2.36	0.49	7.27	NA	NA	NA	0.32
SSAA019	SA019_726A/B	BMZ	Semi-massive/massive	5.30	0.30	1.08	0.42	6.75	2.63	1.50	7.48	0.09
SSAA019	SA019_727	BMZ	Semi-massive/massive (vein)	5.62	0.26	1.28	0.52	7.51	3.01	1.50	7.51	0.15
SSAA019	SA019_729A/B	BMZ	Semi-massive/massive	6.26	0.72	2.55	1.72	11.24	3.51	2.22	17.25	0.17
SSAA019	SA019_749	BMZ	Semi-massive/massive	5.54	1.04	1.55	0.43	0.95	0.07	0.02	0.12	0.17
SSAA019	SA019_750	BMZ	Semi-massive/massive	9.24	1.65	2.76	1.76	1.04	NA	NA	NA	0.49
SSAA029	SA029_761	BMZ	Disseminated/blebby	6.17	2.89	25.60	32.79	19.47	NA	NA	NA	1.50
SSAA034	SA034_769	BMZ	Disseminated/blebby	10.63	4.50	52.39	42.63	3.08	NA	NA	NA	2.05
SSAA034	SA034_772	BMZ	Disseminated/blebby	8.11	4.77	22.45	17.77	NA	NA	NA	NA	0.94
SSAA034	SA034_780	BMZ	Disseminated/blebby	14.33	7.88	34.60	28.42	NA	NA	NA	NA	3.71
SSAA043	SA043_764	Above BMZ	Disseminated/blebby	5.45	2.04	4.13	2.85	NA	NA	NA	NA	0.57
SSAA043	SA043_769	Above BMZ	Disseminated/blebby	NA	NA	NA	NA	NA	NA	NA	NA	NA
SSAA043	SA043_791	BMZ	Disseminated/blebby	7.80	7.12	153.44	174.32	249.56	126.08	81.34	818.94	2.22
SSAA043	SA043_794	Sub-BMZ	Vein	3.88	1.30	17.39	24.82	15.71	NA	NA	NA	1.69

Table 4. *Summary of LA-ICP-MS analysis of trace elements in sulfide in the BM Zone at Sandsloot. BDL = below detection limit. na = no analysis, n = number of analyses (full results are available in Appendix. Table. A4). * = below detection limit, - = no analysis*

Sulfide Texture	Mineral		57Fe wt.%	59Co ppm	61Ni wt.%	63Cu wt.%	75As ppm	77Se ppm	101Ru ppm	103Rh ppm	107Ag ppm	108Pd ppm	121Sb ppm	125Te ppm	189Os ppm
Diss/blebby	po (n =	Average	59.6	30.1	0.22	0.00	*	67.1	14.4	3.62	0.25	0.08	0.18	0.49	1.46
n of samples =	12)	Min	56.2	13.7	0.10	0.00	*	53.2	0.74	*	0.08	*	*	*	0.12
3		Max	65.5	51.9	0.33	0.01	*	85.1	42.7	20.1	0.64	0.25	0.18	0.51	4.68
		2σ	5.64	23.2	0.14	0.01	*	23.3	28.2	12.8	0.30	0.19	*	0.06	2.67
Semi-massive/	po (n=22)	Average	60.5	29.6	0.33	0.00	*	36.9	6.96	0.43	0.15	0.02	0.15	0.11	1.15
massive		Min	55.0	21.0	0.22	0.00	*	27.7	*	*	*	*	*	*	*
n of samples =		Max	68.7	48.4	0.43	0.02	*	47.0	19.1	1.82	0.51	0.02	0.15	0.17	1.81
6		2σ	6.44	16.3	0.10	0.01	*	11.8	10.1	0.91	0.28	0.01		0.18	0.83
Vein	po (n =	Average	60.6	17.3	0.18	0.00	*	51.5	0.56	0.06	0.55	0.09	0.04	0.22	0.13
n of samples =	11)	Min	53.6	13.1	0.03	0.00	*	29.0	0.01	0.01	*	*	*	*	*
2		Max	68.6	20.8	0.35	0.00	*	86.2	1.82	0.12	3.13	0.12	0.07	0.22	0.18
		2σ	11.3	5.56	0.27	0.00	*	29.1	1.36	0.08	1.85	0.08	0.04		0.09
Diss/blebby	pn (n = 6)	Average	31.1	10300	28.6	0.07	1.34	65.0	23.7	116	3.05	346	0.29	1.75	2.20
n of samples =		Min	30.2	9520	23.8	0.00	0.95	55.1	0.72	4.07	1.27	74.4	*	*	0.12
3		Max	33.2	11100	30.3	0.34	1.93	70.8	45.0	244	4.17	657	0.67	1.75	6.81
		2σ	2.30	1230	4.90	0.27	0.84	11.4	31.7	238	1.98	591	0.65		4.84
Semi-massive/	pn (n =	Average	32.4	11100	31.1	0.00	0.56	34.5	8.48	12.2	1.18	10.2	*	1.59	1.24
massive	37)	Min	29.3	8250	25.7	0.00	*	25.6	0.51	0.01	0.15	2.66	*	*	*
n of samples =		Max	37.8	13500	37.8	0.01	1.07	50.9	23.7	62.9	4.45	21.1	*	7.93	4.53
6		2σ	4.56	3060	6.65	0.01	0.53	12.3	13.5	33.2	2.45	8.97	*	4.62	1.95
Vein	pn (n =	Average	33.1	10900	28.2	0.00	0.34	51.1	2.16	18.7	6.42	153	*	1.21	0.12
n of samples =	10)	Min	29.3	8690	26.8	0.00	*	32.8	0.47	0.02	0.20	5.09	*	*	*
2		Max	37.4	12500	29.7	0.00	0.46	87.9	4.03	86.9	18.8	285	*	2.77	0.18
		2σ	6.39	3120	1.73	0.00	0.17	34.9	2.95	52.3	12.9	254	*	2.38	0.11
Diss/blebby	cpy (n =	Average	27.7	9.81	0.04	30.7	*	47.2	-	-	3.18	-	*	0.63	0.90
n of samples =	5)	Min	26.8	0.16	0.00	29.9	*	38.4	-	-	1.34	-	*	*	*
3		Max	28.4	38.0	0.14	31.8	*	64.3	-	-	5.29	-	*	0.63	0.90
		2σ	1.41	31.9	0.11	1.39	*	22.5	-	-	3.56	-	*		
Semi-massive/	cpy (n =	Average	29.8	11.0	0.04	32.3	*	32.2	-	-	1.38	-	*	0.43	0.68
massive	15)	Min	27.0	*	0.00	27.1	*	19.2	-	-	0.30	-	*	*	*
n of samples =		Max	38.1	90.0	0.23	37.6	*	41.2	-	-	2.63	-	*	0.65	1.55
6		2σ	5.89	46.4	0.12	4.53	*	11.9	-	-	1.62	-	*	0.64	1.06
Vein	cpy (n =														
n of samples =	1)		37.5	4.92	0.01	20.0	*	28.3	-	-	2.84	0.78	*	*	*
1															

Table 4. *Continued*

193Ir ppm	195Pt ppm	197Au ppm	208Pb ppm	209Bi ppm
1.53	0.14	0.14	1.72	0.06
0.03	*	*	0.84	*
4.17	0.31	0.29	2.48	0.33
3.09	0.23	0.20	0.99	0.19
0.91	*	0.07	1.81	0.42
0.03	*	*	0.53	0.11
1.94	*	0.18	6.81	1.27
1.38	*	0.13	2.91	0.55
0.17	0.10	0.04	5.09	0.42
0.02	*	*	1.18	*
0.57	0.10	0.08	25.8	1.07
0.42		0.08	14.2	0.73
2.32	2.51	0.11	10.8	0.22
0.48	0.25	*	2.99	0.01
5.23	4.22	0.22	33.3	1.22
3.63	3.49	0.17	22.8	0.98
1.59	*	0.06	4.19	0.39
*	*	*	0.15	0.05
8.15	*	0.15	14.7	1.41
3.86	*	0.08	7.13	0.60
0.58	0.22	0.02	16.8	0.79
*	*	*	2.27	*
1.27	0.30	0.03	43.4	1.38
0.98	0.12	0.03	30.1	1.13
0.09	0.14	0.28	11.2	0.06
*	*	*	7.65	*
0.09	0.15	0.53	16.7	0.08
	0.03	0.45	7.79	0.06
0.32	*	0.07	4.46	0.47
*	*	*	1.97	0.06
1.19	*	0.15	7.09	1.23
0.79	*	0.11	3.43	0.69
0.04	*	0.05	49.9	0.02

Table. 5. *Table summarising the % of PGM and PMM by area and no of grains, alongside their total areas and number (n) of grains. The names and ideal formulas of PGM within each group are also given. Full PGM and PMM datasets are available in Table. A5, A6.*

PGM Group	PGM Name	Ideal formula	% of PGM by total area	% of grains	Total area (μm^2)	Total n of grains
Ru-S	Laurite	(Os, Ir)RuS_2	61.8	27.4	35231	60
Ir-As	Iridarsenite	$IrAs_2$	1.2	19.6	671	43
IPGE+Pt-As-S	Hollingworthite	RhAsS	0.0	2	11	5
	Platarsite	(Pt,Ir,Os)AsS	21.3	5	12136	12
	Irarsite	(Ir,Pt,Os)AsS	0.2	8	89	18
Ir-alloys	IrPbAs unknown	Ir-Pb-As	0.1	0.5	32	1
PPGE-As	Palladoarsenide	$PdAs_2$	0.03	3.2	15	7
	Sperrylite	$PtAs_2$	0.55	2.7	315	7
Pt-Bi-Te	Moncheite	$Pt(Te, Bi)_2$	0.7	6.4	377	14
Pd-Bi-Te	Merenskyite	$Pd(Te,Bi)_2$	0.2	0.9	101	2
Pt-Fe	Isoferroplatinum	Pt_3Fe Pt_2Fe	10.6	8.7	6043	19
Au-Ag	Electrum	(Au-Ag)	3.5	14.6	1985	32